Passive Targeted Energy Transfers and Strong Modal Interactions in the Dynamics of a Thin Plate with Strongly Nonlinear Attachments

Fotios Georgiades
Postdoctoral Researcher
LTAS-Vibration and Identification Group Aerospace and Mechanical Eng. Dept.,
University of Liege, 1 Chemin des Chevreuils (B52/3), 4000, Liege, Belgium,
Fotios.Georgiades@ulg.ac.be

Alexander F. Vakakis
Professor
Dept. of Mechanical Science and Engineering,
University of Illinois, Urbana, IL 61801, avakakis@illinois.edu

Abstract

We study Targeted Energy Transfers (TETs) and nonlinear modal interactions attachments occurring in the dynamics of a thin cantilever plate on an elastic foundation with strongly nonlinear lightweight attachments of different configurations in a more complicated system towards industrial applications. We examine two types of shock excitations that excite a subset of plate modes, and systematically study, nonlinear modal interactions and passive broadband targeted energy transfer phenomena occurring between the plate and the attachments. The following attachment configurations are considered: (i) a single ungrounded, strongly (essentially) nonlinear single-degree-of-freedom (SDOF) attachment – termed nonlinear energy sink (NES); (ii) a set of two SDOF NESs attached at different points of the plate; and (iii) a single multi-degree-of-freedom (MDOF) NES with multiple essential stiffness nonlinearities. We perform parametric studies by varying the parameters and locations of the NESs, in order to optimize passive TETs from the plate modes to the attachments, and we showed that the optimal position for the NES attachments are at the antinodes of the linear modes of the plate. The parametric study of the damping coefficient of the SDOF NES showed that TETs decreasing with lower values of the coefficient and moreover we showed that the threshold of maximum energy level of the system with strong TETs occured in discrete models is by far beyond the limits of the engineering design of the continua. We examine in detail the underlying dynamical mechanisms influencing TETs by means of Empirical Mode Decomposition (EMD) in combination with Wavelet Transforms. This integrated approach enables us to systematically study the strong modal interactions occurring between the essentially nonlinear NESs and different plate modes, and to detect the dominant resonance captures between the plate modes and the NESs that cause the observed TETs. Moreover, we perform comparative studies of the performance of different types of NESs and of the linear Tuned-Mass-Dampers (TMDs) attached to the plate instead of the NESs. Finally, the efficacy of using this type of essentially nonlinear attachments as passive absorbers of broadband vibration energy is discussed.

Key words: Nonlinear targeted energy transfers, nonlinear modal interactions, shock isolation

1. Introduction

Towards industrial applications, we study a thin plate lying on an elastic foundation with essentially nonlinear attachments of different configurations attached to it. We discretize the partial differential equation of motion of the thin plate using a Finite Element (FE) formulation to extract the structural matrices of the system, and then add the essentially nonlinear attachments with different configurations. For the class of systems considered in this work (e.g., a primary linear structure with an essentially nonlinear attachment at its boundary), it has been shown that at certain energy levels there may occur passive targeted energy transfer (TET) phenomena from the primary system to the nonlinear attachment, which acts, in essence as nonlinear energy sink (NES) (Vakakis, 2001). When TET takes place, there occurs passive, broadband, directed (on the average) energy transfer from the primary, directly excited structure to the NES (that is initially at rest), where this energy gets localized (spatially confined) and locally dissipated without major backscattering to the primary structure.

In previous works the dynamical mechanisms governing passive TET have been studied; these include nonlinear beat phenomena, and fundamental and subharmonic resonance captures between the linear part and the NES attachment (Gendelman et al., 2001; Vakakis and Gendelman, 2001; Kerschen et al., 2005; Lee et al., 2005).

The present work aims to systematically study the nonlinear modal interactions and compare passive broadband targeted energy transfer (TET) phenomena between the linear dispersive plate and the following configurations of NES attachments: (i) a single ungrounded, strongly (essentially) nonlinear single-degree-of-freedom (SDOF) NES; (ii) multiple nonlinear SDOF NESs attached at different points of the plate; (iii) a single, multi-degree-of-freedom (MDOF) NES with essential stiffness nonlinearities; and (iv) a single Linear Tuned Mass Damper (TMD) attachment to the plate. We examine conditions for optimal TETs from the plate to the attached NESs, and we compare the performance of the different NESs to linear TMDs.

In these studies we examined TETs with two different types of input force applied to the plate, either a single shock that directly excites at least the five leading plate modes, or multiple shocks that excite equivalently, at least three leading plate modes. We examine the capacity of the NESs to passively absorb and locally dissipate broadband shock energy from the plate. What clearly distinguishes this work from other TET studies is the systematic study of transient, strongly nonlinear TET in an elastic continuum – NES system of far more complicated configuration that those these examined in the literature thus far –towards industrial applications-, the parametric study of TETs with the applied amplitude of the force within the design limits of the linear structure, the comparative studies of TETs between different NESs, TMD attachments and different types of forces that excites higher than the three first modes of the linear system.

In related works on elastic continua with attached NESs, Georgiades and Vakakis (2007) have studied numerically TETs from a beam to a SDOF NES attachment, and found conditions for optimal TET; in that work as much as 87% of the shock energy of the beam could be transferred and locally dissipated by the NES. Georgiades et al. (2007) have studied TETs from a dispersive rod (linearly elastic rod on an elastic foundation) to a SDOF NES attachment. In that work Wavelet transforms and Empirical Mode Decomposition (EMD) were used to analyze the nonlinear resonance captures that govern TET in that system. TET from a dispersive rod under shock excitation to an attached MDOF NES at its boundary was studied in (Tsakirtzis et al., 2007). In an earlier work (Tsakirtzis et al., 2005) the dynamics and TET in discrete oscillators with an attached MDOF NES have been studied. The present work aims to extend these previous results, by studying TET and complex nonlinear modal

interactions of an elastic system with more complicated configuration with essentially nonlinear attachments.

2. Finite Element (FE) Formulation for the Plate Dynamics and Different NES Configurations

The plate on the linear elastic foundation is depicted in Figure 1a. It consists of a linear isotropic elastic plate with mass distribution per unit area M, width W, length L, thickness h, and distributed proportional viscous damping per unit area d (this corresponds either to distributed viscous damping in the foundation or to Rayleigh damping in the plate with β=0). The plate is clamped on one edge only, with all other edges remaining traction-free, and is resting on a distributed elastic foundation with stiffness per unit area equal to K. The plate is assumed to be sufficiently thin, so that its shear deformation may be neglected (the so called Kirchhoff assumptions). Hence, the governing partial differential equation of motion with the associated boundary conditions is given by (assuming that the plate is initially at rest):

$$\begin{gathered} D\nabla^4 w + M\frac{\partial^2 w}{\partial t^2} + d\frac{\partial w}{\partial t} + k\,w + F_{ext,1}\delta(x-d_{x_1}, y-d_{y_1}) + F_{ext,2}\delta(x-d_{x_2}, y-d_{y_2}) = \\ \sum_i F_i(t)\,\delta(x-b_{x_i}, y-b_{y_i}) \\ w(x,0,t)=0,\ \frac{\partial w(x,0,t)}{\partial x}=0,\ w(x,y,0)=0,\ \frac{\partial w(x,y,0)}{\partial t}=0 \\ M_y(0,y,t)=M_y(W,y,t)=M_y(x,L,t)=0 \\ Q_y(0,y,t)=Q_y(W,y,t)=Q_y(x,L,t)=0 \end{gathered} \tag{1.1}$$

Depending on the specific forms of the forcing terms in (1.1) we will consider different models as outlined below:

Model 1: Simple plate without attachments: $F_{ext,1}=F_{ext,2}=0$ (1.2)

Model 2: Plate with SDOF NES attachment:

$$F_{ext,1} = C\left[w(d_{x_1},d_{y_1}) - v(t)\right]^3 + \lambda\left[\dot{w}(d_{x_1},d_{y_1}) - \dot{v}(t)\right] \tag{1.3}$$

$$F_{ext,2} = 0 \tag{1.4}$$

$$\varepsilon\ddot{v}(t) + C\left[v(t) - w(d_{x_1},d_{y_1})\right]^3 + \lambda\left[\dot{v}(t) - \dot{w}(d_{x_1},d_{y_1})\right] = 0,\ v(0)=0,\ \dot{v}(0)=0 \tag{1.5}$$

Model 3: Plate with Multi-SDOF NES attachment:

$$F_{ext,1} = C\left[w(d_{x_1},d_{y_1}) - v(t)\right]^3 + \lambda\left[\dot{w}(d_{x_1},d_{y_1}) - \dot{v}(t)\right] \tag{1.6}$$

$$F_{ext,2} = C\left[w(d_{x_2},d_{y_2}) - s(t)\right]^3 + \lambda\left[\dot{w}(d_{x_2},d_{y_2}) - \dot{s}(t)\right] \tag{1.7}$$

$$\varepsilon\ddot{v}(t) + C\left[v(t) - w(d_{x_1},d_{y_1})\right]^3 + \lambda\left[\dot{v}(t) - \dot{w}(d_{x_1},d_{y_1})\right] = 0,\ v(0)=0,\ \dot{v}(0)=0 \tag{1.8}$$

$$\varepsilon\ddot{s}(t) + C\left[s(t) - w(d_{x_2},d_{y_2})\right]^3 + \lambda\left[\dot{s}(t) - \dot{w}(d_{x_2},d_{y_2})\right] = 0,\ s(0)=0,\ \dot{s}(0)=0 \tag{1.9}$$

Model 4: Plate with MDOF NES attachment:

$$F_{ext,1} = C_0\left[w(d_{x_1},d_{y_1}) - v(t)\right] \tag{1.10}$$

$$F_{ext,2} = 0 \tag{1.11}$$

$$m_1\ddot{v}(t) + C_0\left[v(t) - w(d_{x_1},d_{y_1})\right] + \lambda\left[\dot{v}(t) - \dot{u}(t)\right] + C_1\left[v(t) - u(t)\right]^3 = 0,\ v(0)=0,\ \dot{v}(0)=0 \tag{1.12}$$

$$m_2\,\ddot{u}(t)+\lambda\left[\dot{u}(t)-\dot{v}(t)\right]+C_1\left[u(t)-v(t)\right]^3+$$

$$+\lambda\left[\dot{u}(t)-\dot{s}(t)\right]+C_2\left[u(t)-s(t)\right]^3=0,\ u(0)=0,\ \dot{u}(0)=0 \qquad (1.13)$$

$$m_3\,\ddot{s}(t)+\lambda\left[\dot{s}(t)-\dot{u}(t)\right]+C_2\left[s(t)-u(t)\right]^3=0,\ s(0)=0,\ \dot{s}(0)=0 \qquad (1.14)$$

Model 5: Plate with TMD attachment:

$$F_{ext,1}=k_{ln}\left[w(d_{x_1},d_{y_1})-v(t)\right]+\lambda\left[\dot{w}(d_{x_1},d_{y_1})-\dot{v}(t)\right] \qquad (1.15)$$

$$F_{ext,2}=0 \qquad (1.16)$$

$$\varepsilon\,\ddot{v}(t)+k_{ln}\left[v(t)-w(d_{x_1},d_{y_1})\right]+\lambda\left[\dot{v}(t)-\dot{w}(d_{x_1},d_{y_1})\right]=0,\ v(0)=0,\ \dot{v}(0)=0 \qquad (1.17)$$

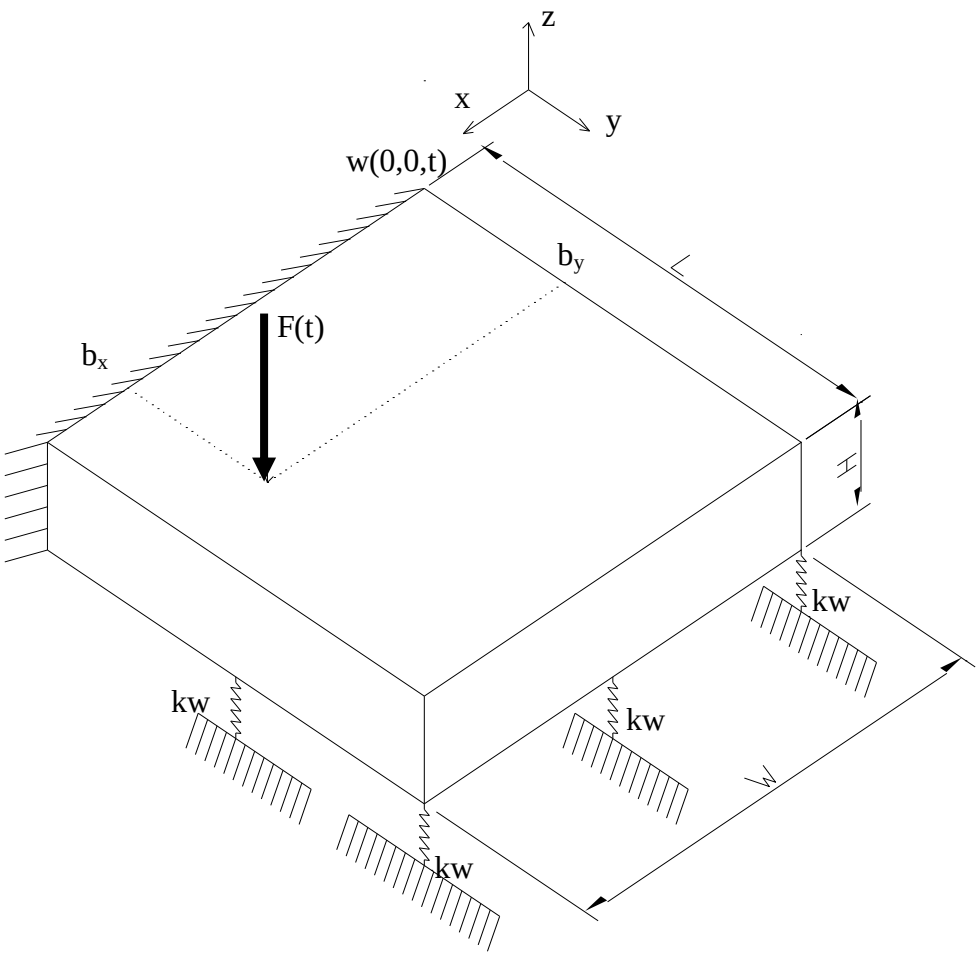

(a)

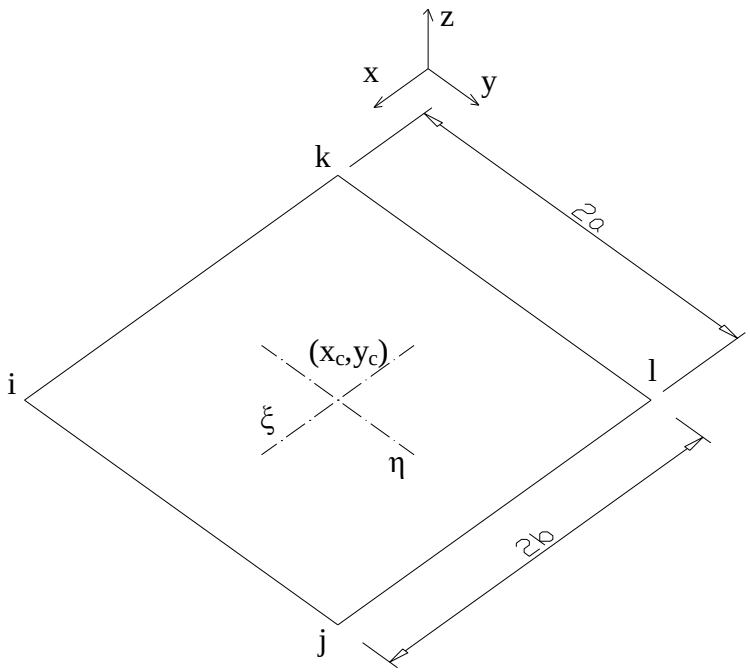

(b)

Figure 1. Cantilever plate with elastic foundation: (a) Configuration of the plate, (b) the 4-node quadrilateral finite element indicating the local coordinates (ξ, η).

In these models $F(t)$ is the applied external excitation, $\delta(\cdot,\cdot)$ is Dirac's generalized function, and the differential operator ∇ applies to both x and y directions. In (1) the variables $M_y(\cdot,\cdot)$ and $Q_y(\cdot,\cdot)$ denote the internal bending moments about the y-axis, and the shear forces along the y-axis of the plate, respectively (cf. Figure 1). Moreover, the flexibility D in the equation of the plate is defined as,

$$D = \frac{Eh^3}{12(1-\nu^2)} \tag{2}$$

where E is the modulus of elasticity, and ν is Poisson's ratio for the material of the plate (Leissa, 1993).

Equations (1.1) and (1.2) have been nondimensionalised, with the following numerical values assigned for the plate parameters,

$$W = L = 1,\ h = 0.01,\ M = 1,\ D = 1,\ \nu = 0.3,\ k = 100 \tag{3}$$

which are in accordance to the assumptions of thin plate theory; the damping coefficient is assigned the value d=0.10 for the case of a single force (shock) applied to the plate, and d=0.15 for the case of multiple forces applied to the plate, in order to perform comparative studies of TET efficiency between various configurations of NESs and linear tuned mass dampers (TMDs). In SDOF NES configurations a single mass is attached to the plate by means of an essentially nonlinear stiffness in parallel to a viscous damper. In MDOF NES configurations a 3-DOF NES system is connected to the plate through a linear coupling stiffness without a dissipative element; also, two essentially nonlinear stiffness elements in parallel to two viscous damping elements are used to connect the three masses of the MDOF NES. In all cases, the masses of the NESs are assumed to oscillate transversely with respect to the plate.

Additionally, we assume that at $t = 0$ a single or a set of transient forces (shocks) $F_i(t)$ is applied to the plate. Each shock has the form of a half sine impulse:

$$F_i(t) = \begin{cases} A_i \sin(2\pi t / T), & 0 \le t \le T/2 \\ 0, & t > T/2 \end{cases} \tag{4}$$

In the case of a single applied shock, its position on the plate is given by, $(b_x, b_y) = (1,1)$; whereas, in the case of multiple applied shocks, their positions on the plate are given by, $(b_{x1}, b_{y1})=(0.6,0.5)$ (shock 1), $(b_{x2}, b_{y2}) = (0.5,0.5)$ (shock 2) and $(b_{x3}, b_{y3}) = (0.4,0.5)$ (shock 3).

Unless otherwise stated, in the following computations for single forcing the amplitude of the force is selected as, A=100, with period $T = 0.1 \times T_5$, where T_5 is the period of the fifth eigenmode of the linear plate (e.g., the plate with no attachment). This requirement ensures that the applied shock excitation has sufficiently small duration compared to the period of the first eigenmode of the plate, which can be regarded as the characteristic time scale of the problem; in turn, this ensures that the applied shock directly excites a sufficiently large number of eigenmodes of the plate (in this case the first five), which enables us to study the capacity of the NES(s) to passively absorb broadband vibration energy from multiple plate modes. Alternatively, in the case of multiple applied shocks, the forcing amplitudes are selected as, $A_1 = 25$, $A_2 = -100$, and $A_3 = 25$ with period $T = 0.1 \times T_5$, where T_5 is the period of the fifth eigenmode of the linear plate, and examination of the response at the free corner of the simple plate with wavelet spectra showed that there are three excited modes with almost equivalent energy (the 1st, 4th and 6th modes).

The partial differential equation in (1.1) with (1.2) is discretized using a 4-node quadrilateral element, as well as non-conforming shape functions with corner nodes (with 12 degrees of freedom) (Zeinkiewicz and Taylor, 2000; Liu and Quek, 2003). In each node, we consider the transverse displacement (w) and the rotations over the x and y axis. For this specific finite element, the explicit forms of the matrix of shape functions, N, was derived by Melosh (1963), and expressed simply in terms of local normalized coordinates (ξ,η) at each node as follows (Zeinkiewicz and Taylor, 2000),

$$(N_p^m)^T = \begin{Bmatrix} N_p^1 \\ N_p^2 \\ N_p^3 \end{Bmatrix} = \frac{1}{8}(1+\xi_0)(1+\eta_0) \begin{Bmatrix} 2+\xi_0+\eta_0-\xi^2-\eta^2 \\ b\eta_p(1-\eta^2) \\ -\alpha\xi_p(1-\xi^2) \end{Bmatrix} \tag{5}$$

where p(=i,j,k,l) is the number of node and (m) is the index denoting to which element of the vector q_p does the shape function correspond; the local coordinates are defined as,

$$\xi = \frac{x - x_c}{\alpha}, \quad \xi_0 = \xi\xi_p \tag{6}$$

$$\eta = \frac{y - y_c}{b}, \quad \eta_0 = \eta\eta_p \tag{7}$$

where ξ_p and η_p are the local coordinates for node p, and (x_c, y_c) denote the coordinates of the center of the finite element (cf. Figure 1b).

There are several ways to discretize the partial differential equation in (1.1) with (1.2). In this work we found more convenient to use the energy approach based on the estimation of energies of a single finite element from Kirchoff's plate theory, and using the results to estimate the corresponding FE mass matrices and FE displacements. Using a connection matrix that indicates which nodes are connected in adjacent elements we may construct the full structural matrices of the plate as follows (see details in Appendix 1):

$$K^{I,II} q + M_d \ddot{q} + D\dot{q} = P(t) \tag{8}$$

In (8) q is a column vector containing the vertical displacement and the rotations about the x and y axis at each node; M_d is the mass structural matrix and $K^{I,II}$ is the

stiffness matrix; and P(t) is a column vector with zero elements, except for nodes where excitations forces (shocks) are applied. In equation (1) proportional distributed viscous damping is considered; hence, in the discrete model (8) the damping matrix D appears, which is proportional to the mass matrix M_d (see details in Appendix 1).

The discrete system (8) was solved numerically using the Newmark Adaptive Algorithm [for details see (Geradin and Rixen, 1997)]. A sensitivity analysis for the required number of discrete elements needed for convergence showed that a total of 10×10 elements (10 in each direction) was sufficient. Initially a verification of the accuracy of the natural frequencies was performed for the case of no elastic foundation (k=0) using a model in ANSYS, and comparing with the results reported in (Leissa, 1993). In Table 1 we present the natural frequencies for the unforced and undamped plate estimated using the FE simulation, together with the corresponding eigenshapes and for comparison purposes there are the eigenfrequencies arised by Leissa (1993) that shows good agreement with the determined values.

Table 1. FE computations of the leading eigenmodes of the plate on elastic foundation (k=100), with no NES attached.

Eigenmode No.	1	2	3
Eigenfrequency (Leissa 1993)	1.686	2.093	3.765
Eigenfrequency (Hz)	1.685	2.090	3.750
% Critical damping ratios for d=0.10	0.472	0.381	0.212
% Critical damping ratios for d=0.15	0.708	0.571	0.319
Eigenshapes- Nodal Lines (.....)	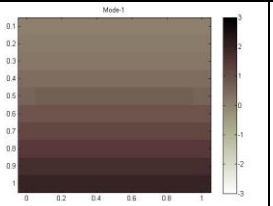	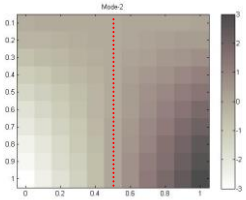	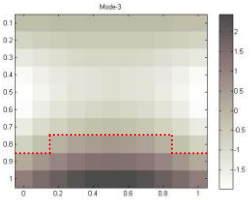

Eigenmode No.	4	5
Eigenfrequency (Ref. Leissa 1993)	4.651	5.209
Eigenfrequency (Hz)	4.607	5.179
% Critical damping ratios for d=10	0.173	0.154
% Critical damping ratios for d=15	0.259	0.230
Eigenshape	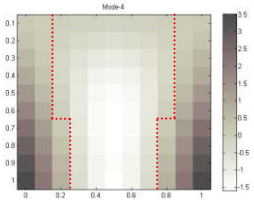	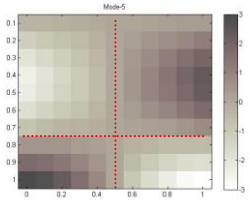

We now assume that a single essentially nonlinear attachment (referred to from now on as 'nonlinear energy sink' – NES) is attached at position (x,y) = (d_x,d_y) of the plate, model 2 with equations (1.1,1.3-1.5). The NES is assumed

to be lightweight – of mass ε, and to possess an essentially nonlinear (nonlinearizable) cubic stiffness with characteristic C, in parallel to a viscous damper λ.

The partial differential equation in (1.1) was discretized using the aforementioned FE formulation, and the dynamics of the NES at $(x,y) = (d_x,d_y)$ is incorporated into the discretized equations of motion by expanding accordingly the system matrices, and adding a nonlinear stiffness component (due to the essential cubic nonlinearity).

The efficiency of the NES to passively absorb and locally dissipate the shock energy of the plate, can be studied by estimating the following energy dissipation measure (EDM):

$$\eta(t) \equiv \frac{E_{damp,NES}(t)}{E_{in}} = \frac{\lambda \int_0^t \left[\dot{w}(d_x, d_y, \tau) - \dot{v}(\tau) \right]^2 d\tau}{\int_0^t F(\tau)\, \dot{w}(b_x, b_y, \tau) d\tau} \tag{9}$$

This represents the portion of the shock energy of the plate that is dissipated by the damper of the NES at time t, and hence, can be used as a measure of TET efficiency. It is clear that with increasing time the EDM reaches an asymptotic limit,

$$\eta_{t>>1} = \lim_{t>>1} \eta(t) \tag{10}$$

which represents the portion of the shock energy of the plate that is *eventually* dissipated by the NES by the end of the oscillation.

The portion of the input shock energy dissipated by the distributed viscous damping of the plate up to time instant t is computed by,

$$\eta_{plate}(t) \equiv \frac{E_{damp,plate}(t)}{E_{in}} = \frac{\frac{1}{2} \int_0^L \int_0^W \int_0^t d\left[\frac{\partial w(x,\tau)}{\partial \tau} \right]^2 d\tau\, dx\, dy}{\int_0^t F(\tau)\, \dot{w}(b_x, b_y, \tau)\, d\tau} \tag{11}$$

Combining (9) and (11), the portion of the input shock energy dissipated by the integrated plate-NES system up to time instant t is computed as follows,

$$\eta_{total}(t) = \eta(t) + \eta_{plate}(t) \tag{12}$$

Similar formulations hold when multiple SDOF NESs or the linear TMD and the equations of motion for the integrated plate – Multi SDOF NES system considered in this work are given by model 3 equations (1.1, 1.6-1.9) and for the integrated plate-TMD system considered in this work are given by model 5 equations (1.1, 1.15-1.17).

Some remarks are now appropriate concerning the use of MDOF NES attachments. In (Tsakirtzis et al., 2005; 2007) a MDOF NES composed of three masses coupled by essentially nonlinear springs and dampers was attached to a system of linear coupled oscillators. This MDOF NES configuration was introduced due to its capacity to passively absorb broadband shock energy from a linear system with enhanced effectiveness and robustness compared to SDOF NESs and an easily realizable attachment in an existing structure by a common linear spring.. The enhanced efficiency of the MDOF NES is attributed to the complex nonlinear modal interactions (and, hence, transient resonance captures) that occur between multiple nonlinear modes of the NES and linear modes of the system to which it is attached; for example, MDOF NESs were shown to be effective in passive energy absorption even in low-amplitude regimes (Tsakirtzis et al., 2007), in contrast to SDOF NESs which are 'activated' only above a definite energy threshold. These results provide us with the motivation to test the performance of the MDOF NES to the present problem of plate vibration.

The equations of motion for the integrated plate – MDOF NES system considered in this work are given by model 4 equations (1.1, 1.10-1.14). The MDOF NES attachment is consists of three masses coupled together with nonlinear spring and damper with the same damping coefficinet and the third mass coupled with the plate by linear spring.

Details of the FE formulation and the corresponding structural matrices of the integrated system can be found in Appendix 1. The effectiveness of the NES to passively absorb and locally dissipate the shock energy of the plate (e.g., the TET efficiency) can be quantitatively studied by computing the following energy dissipation measures (EMDs),

$$\eta_1(t) \equiv \frac{E_{damp,NES_1}(t)}{E_{in}} = \frac{\lambda \int_0^t \left[\dot{u}(\tau) - \dot{v}(\tau)\right]^2 d\tau}{\int_0^t F(\tau)\ \dot{w}(b_x, b_y, \tau) d\tau} \tag{13}$$

and

$$\eta_2(t) \equiv \frac{E_{damp,NES_2}(t)}{E_{in}} = \frac{\lambda \int_0^t \left[\dot{s}(\tau) - \dot{u}(\tau)\right]^2 d\tau}{\int_0^t F(\tau)\ \dot{w}(b_x, b_y, \tau) d\tau} \tag{14}$$

e.g., the portion of shock energy dissipated by each of the two dampers of the MDOF NES at time t. The summation of these two EMDs provides a measure of the TET efficiency of the MDOF NES. It is clear that the two EMDs reach asymptotic limits, $\eta_{1,2\,t>>1} = \lim_{t>>1} \eta_{1,2}(t)$.

3. Methods of Post-processing the Computational Results

The results of the simulations are post-processed based on energy and frequency points of view. From the energy point of view, we examine the energy dissipation in the system and especially the amount of energy that each part of the system (the elastic continuum and the attachment) is dissipating. Moreover in certain simulations we examine the energy transaction (E_{Trans} – the ratio $E_{Trans}/\Delta t$ when Δt tends to zero represents the power flow from the plate to the attachment and vice versa) between the plate and the attachment at any given instant of time.

Post processing of the numerically computed time series of the plate and the NES was performed in two different ways as discussed in (Georgiades et al., 2007). First, the dynamic response was analyzed using a Wavelet Transform (WT) employing a Matlab code developed in University of Liege by Dr. V. Lenaerts in collaboration with Dr. P. Argoul from the 'Ecole Nationale des Ponts et Chaussees'. In this work, the Morlet motherwavelet was used for the WT computations; that is a Gaussian-windowed complex sinusoid of frequency ω_0 (in rad/sec), $\psi_M(t) = e^{-t^2/2} e^{j\omega_0 t}$. The frequency ω_0 (or f_0 in Hz) is the user parameter that enables one to tune the frequency and time resolution of the results. Using this tool we can extract the Wavelet Transform Spectra that are contour plots depicting the amplitude of the WT of the signal as function of frequency (vertical axis) and time (horizontal axis) (Lee et al., 2005; Kerschen et al., 2005).

Further analysis of the numerical responses was performed using a combination of the Empirical Mode Decomposition (EMD) with Hilbert transform. EMD is a method to decompose a signal in monofrequency oscillatory modes called *Intrinsic Mode Functions (IMFs)* (Huang et al., 1998; 2003; Veltcheva and Soares, 2004; Zhang et al., 2005). In essence, IMFs are oscillatory modes embedded in the time series, and their

linear superposition regenerates the time series. By Hilbert transforming the set of IMFs one computes their instantaneous phases and frequencies. By post processing the transient responses of the plate and the attached NES by means of EMD and Hilbert transform, we aim to study in detail the complex nonlinear resonance interactions taking place between the essentially nonlinear attachment and the various modes of the plate. By combining the results of the Hilbert transform with the corresponding wavelet spectra of the transient responses, we can identify the dominant IMFs of the plate and NES transient responses, and further on analyze the most important modal resonance interactions between the plate and the NES that are responsible for the nonlinear energy exchanges (and TET) between these two subsystems. Details of the EMD method with Hilbert transform and their applications for the determination of the resonance captures between elastic continua and the NES attachments could be found in the PhD Thesis by Georgiades (2006) and also in Georgiades et al., 2007.

In the following sections all the simulations were performed for a sufficiently large time window so at least 96.5% of the energy of the system has been dissipated by the dampers of the subsystems. This total dissipated energy measure (termed η_{total}) ensured that no essential dynamics was missed in the transient simulations due to insufficient time of numerical integration. All sets of simulations with SDOF nonlinear attachments were performed with using a (10×10) FE mesh for the plate. In the presented results we divide the plate in 'y-slices' corresponding to fixed values of y to present the dynamics. The parametric studies of the plate with MDOF attachments were performed with attachments located all over x-positions on three 'y-slices,' namely, y = 1, 0.7, 0.3 of the plate, again using a (10×10) FE mesh.

4. Parametric Studies of TET from the Plate to a SDOF NES

In our first parametric study we examine TET in a plate forced by single or multiple shocks, possessing a single SDOF NES attachment. We perform four main sets of FE simulations with parameter values for the integrated plate – SDOF NES system, model 2 with equations (1.1, 1.3-1.5). In these sets of simulations we examine the influence of the variation of the NES parameters and input energy on the targeted energy transfers (TETs) from the plate to the NES, using as criterion of NES effectiveness (and efficiency) the portion of total energy eventually dissipated by the NES (e.g., the energy dissipation measure – EDM), $\eta_{t>>1} = \lim_{t>>1} \eta(t)$ defined by (10). Hence, from now on, TET efficiency will be judged by the asymptotic value $\eta_{t>>1}$. Unless otherwise stated, the mass of the NES is taken as $\varepsilon = 0.05$, its nonlinear stiffness characteristic as C=1000, and its damping coefficient as λ=0.1.

In the first set of simulations we examined the influence of the nonlinear stiffness coefficient C, and of the position of the NES on the TET efficiency from the plate to the NES. For each simulation we determined the % of instantaneous total energy of the system over the input energy in order to have a measure of the error of the determined energy of the system in cases that the maximum and the minimum of the % of the total energy values is not in acceptable range we increased the sampling frequency and repeat the simulations. For the simulations with single forcing the sampling frequency used is 441.5 Hz that corresponds to a Nyquist frequency of 220 Hz (10 times more than the frequency of the 15th linear mode which is equal to 22.075 Hz). The minimum and maximum values of the instantaneous total energy of the system (including the energy dissipated by the dampers) at each time step of the performed simulations were 99.07% and 100.4% of the applied shock energy, indicating accuracy of the computations. For the simulations with multiple applied shocks the sampling frequency was chosen as 800 Hz corresponding to a Nyquist frequency of 400 Hz (18 times more than the frequency of the 15th linear mode that is 22.075 Hz); the corresponding bounds

of the instantaneous energy for all performed simulations were 99.97% and 100.00%, which indicates that the total energy (including energy dissipated by damping) was appliximately conserved at each time step of the numerical simulations. In Figures 2a,b we depict the asymptotic limit of energy dissipation measure (EMD), $\eta_{t>>1}$, as function of C, and the x-position of the NES on the 'slice' y = 1. In Figure 2a (with $C \in [100, 3000]$) the results of simulations with single shock excitation are depicted, whereas in Figure 2b (with $C \in [100, 1000]$) the results for multi-shock excitation are depicted; for the simulations depicted in Figure 2b the mass of NES was fixed to a smaller value ε = 0.005.

Judging from these results we conclude that for a fixed x-position of the NES the TET effectiveness of the NES is robust in variations of C, for C is in the range $O(10^2)$ - $O(10^3)$. Moreover, the variation of the x-position of the NES on a fixed 'y-slice' affects strongly the TET efficiency; this sensitivity can be explained by the fact that certain locations of the NES may be close to nodal curves of the different modes of the plate, in which case the capacity of the NES to passively absorb and dissipate energy from these particular modes is greatly diminished.

This becomes clear when we depict the TET efficiency of the NES as function of the (x,y) coordinates of the NES, for fixed values of C, cf. Figure 3; we note that the maximum efficiency of the NES damper occurs for positions of the NES at the corners of the plate, with maximum values of $\eta_{t>>1}$ reaching levels of 87.72% and 89.28%, for (x,y) = (0,1) and (x,y) = (1,1), respectively.

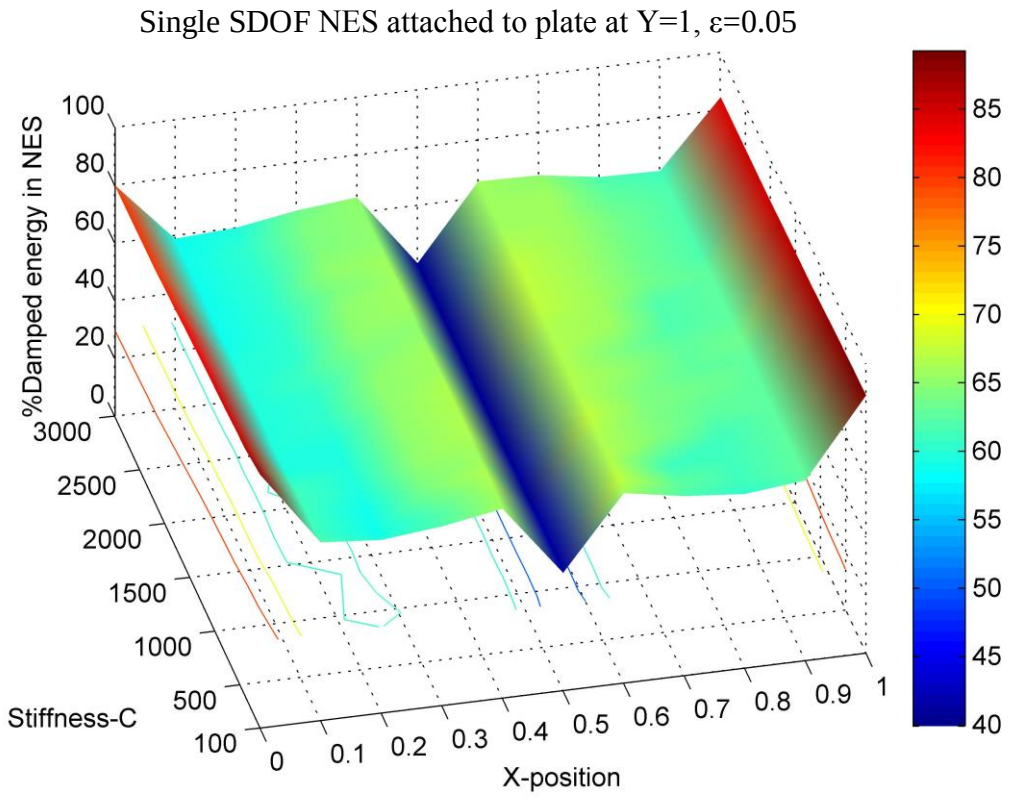

Figure 2a

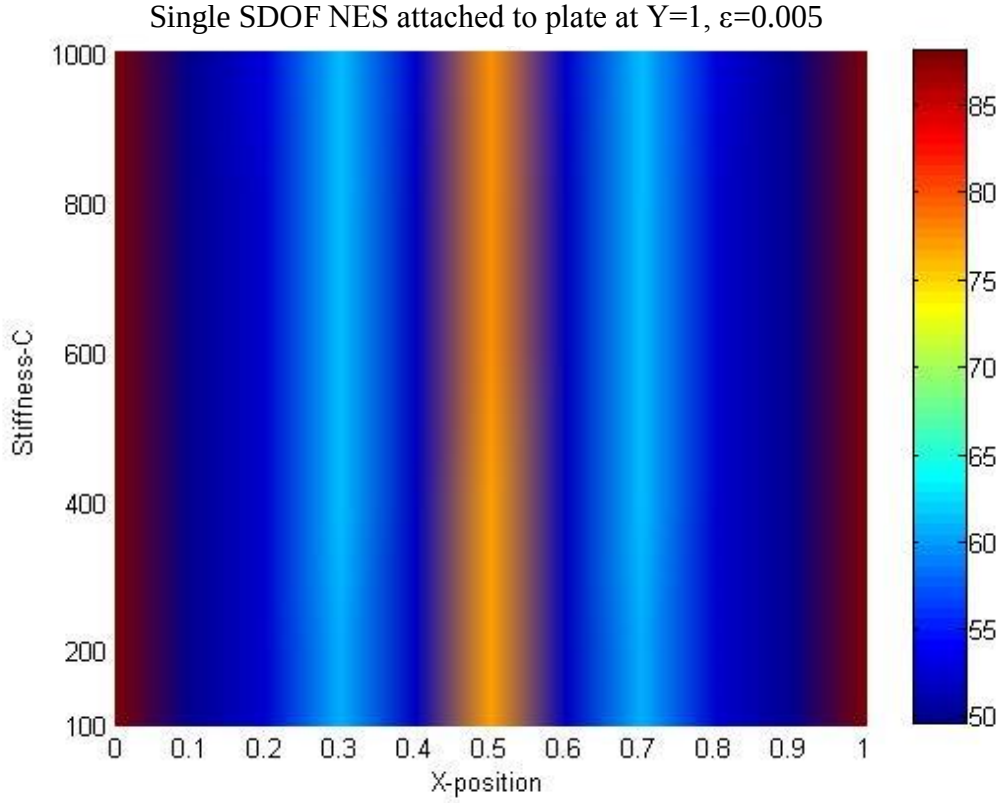

Figure 2b. Parametric study of TET efficiency as function of NES stiffness C, and x-position on the plate for the 'y-slice' y = 1: (a) Case of single shock with NES mass ε=0.05, and (b) case of multiple shocks with NES mass ε=0.005.

The interpretation of the results depicted in this Figure 3 (which correspond to single shock excitation) must be performed in conjunction with the results of Table 1, which depicts the nodal curves of the five leading modes of the linear cantilever plate (with no NES attached). Note that in the strips close to the 'y-slices' y = 0.8 and y = 0.9 (adjacent to the end of the plate and corresponding to the nodal lines of the 3rd and 5th plate modes) the NES efficiency is low; this is due to the fact that when the NES is attached at points in these regions, its capacity to passively absorb and dissipate energy from these modes is impaired. Similarly, at strips positioned close to x = 0.2, x = 0.3, x = 0.7, and x = 0.8, the NES efficiency is relatively low (of the order of 40%); again, this can be interpreted by the fact that these strips are in neighborhoods of nodal curves of the 4th mode of the plate. Finally, there is a strip in the middle of the plate (e.g., for x = 0.5) where the lowest NES efficiency is observed; this is reasonable, given that this region is in the neighborhood of nodes of the 2nd and 5th modes of the plate.

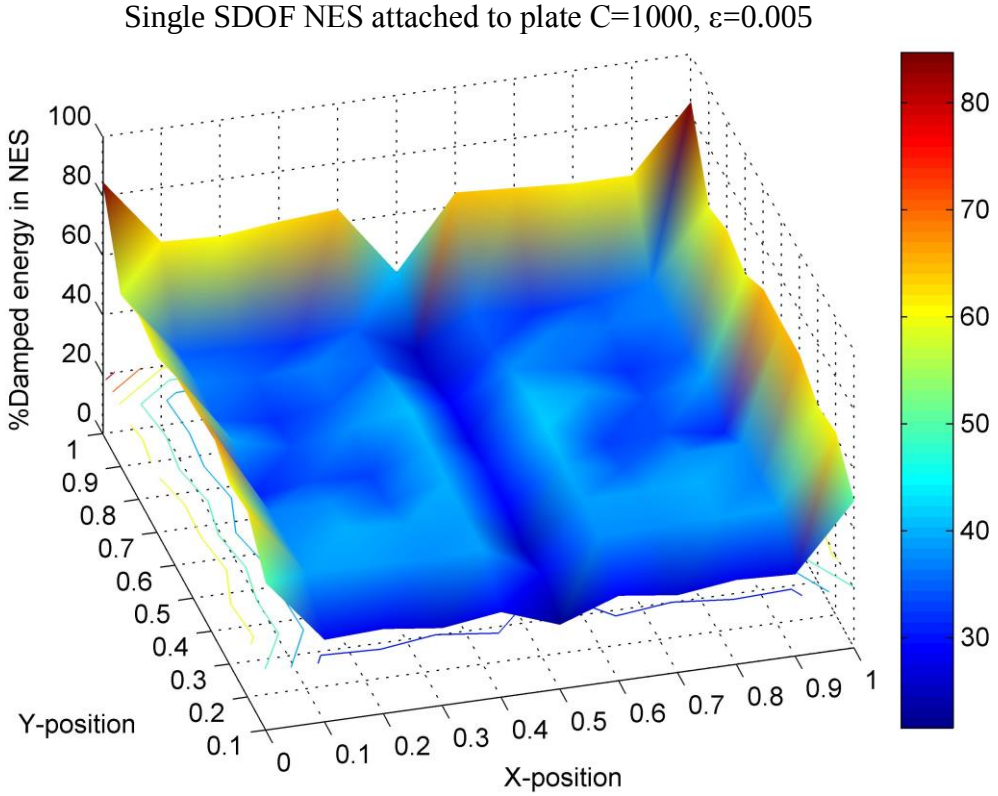

Figure 3. Parametric study for TET efficiency as function of NES position on the plate for C=1000 and NES mass ε=0.005; the clamped boundary condition is at 'y-slice' y = 0.

Moreover, as depicted in Figure 3 the efficiency of the NES decreases when the NES is located closer to the clamped end where the displacements of the plate are reduced and the nonlinear effects are diminished.

In the second set of simulations we consider single shocks applied to the plate, and examine the influence of the NES mass, ε, on the efficiency of the NES, when it is attached at every possible position on the plate. For the second set of simulations with single forcing the sampling frequency used is 441.5 Hz corresponding to a Nyquist frequency of 220 Hz (10 times more than the frequency of the 15th linear mode that is 22.075 Hz); the instantaneous energy of the system (including the energy dissipated by the dampers) is between 99.34% and 100.50% of the applied shock energy at each time step of the simulations, which demonstrates the accuracy of the numerical results. In addition, we examine in more detail the TET efficiency when the NES is attached at the position corresponding to optimal TET, in order to identify the threshold of NES mass below which the TET efficiency starts to deteriorate; similar critical mass thresholds were detected in previous works focusing on linear coupled oscillators with SDOF NESs attached [see for example, (Kerschen et al., 2005)]. In Figure 4a we depict the asymptotic value of the EDM, $\eta_{\tau>>1}$, as function of the mass of the NES ($\varepsilon \in [0.005, 0.1]$), and its x-position on the 'y-slice' y=1. We note that for each x-position of the NES, its effectiveness appears to be robust for variations of its mass. For a SDOF NES located at position (x,y)=(0,1), which is the optimal position for TET (away from the excitation point), we perform an additional series of simulations in order to identify the threshold value of NES mass below which the TET efficiency starts to deteriorate. In Figure 4b we depict the plot of TET efficiency for varying NES mass; from this plot we conclude that the efficiency of the NES is high, even for small values of mass, and that there is a threshold of the NES mass between 3×10^{-4} and 4×10^{-4} below which the TET efficiency is less than 65%. This

indicates that even very lightweight NESs (of the order of 0.04% of the plate mass) can be efficient passive shock absorbers with efficiency more than 65%. As in the first set of simulations, we note that when the NES is located at positions close to nodal lines of plate modes, its efficiency is significantly diminished.

In the third set of numerical simulations, single shocks are applied to the plate, and we examine the influence of the damping coefficient λ on the efficiency of the NES, when it is attached at every possible position on the plate. For the third set of simulations the sampling frequency used is 441.5 Hz that corresponds to Nyquist frequency of 220 Hz (10 times more than the frequency of the 15th linear mode that is 22.075 Hz) with instantaneous total energy being between 97.49% and 100.30% of the applied shock energy. In Figure 5 we depict the asymptotic EDM value $\eta_{\tau>>1}$, as function of the NES damping coefficient, λ ($\lambda \in [0.01, 0.5]$), and the x-position of the NES for a representative 'y-slice' corresponding to y=1. We note a deterioration of NES efficiency with decreasing damping coefficient. This trend, however, does not necessarily mean that by indefinitely increasing NES damping to larger values we will achieve a corresponding monotonic increase of NES efficiency. Indeed, for sufficiently large values of NES damping the *relative motion* between the NES and the plate is expected to significantly decrease (as the connection between the plate and the NES becomes more rigid), which, in turn, will result to a decrease of the relative motion across the damper of the NES, and, hence, to a decrease of the capacity of the NES damper to dissipate shock energy; this will lead to a deterioration of NES efficiency.

In the final set of simulations of this series, we examine the influence of the input energy and the nonlinear stiffness characteristic C on the performance of the NES, when it is located at position (x,y)=(0.1) of the plate. A single shock is assumed to apply to the plate and the NES mass is ε=0.005. For this set of simulations the sampling frequency used is 800 Hz that corresponds to Nyquist frequency of 400 Hz (18 times more than the frequency of the 15th linear mode that is 22.075 Hz) with instantaneous total energy being between between 97.67% and 100.03% of the applied shock energy. We can determine the range of energies that of practical (engineering) interest, e.g., the range of energies for which the vibration of the plate is of interest from an engineering point of view; hence, we examine shock amplitudes in the range $A \in [0.001, 100]$ (input energy) for which the plate without NES is vibrating with maximum absolute displacement within the range $\max[\text{abs}(w)] \in [9.7\times10^{-6}, 0.97]$ (note that the linear dimensions of the plate are normalized to 1).

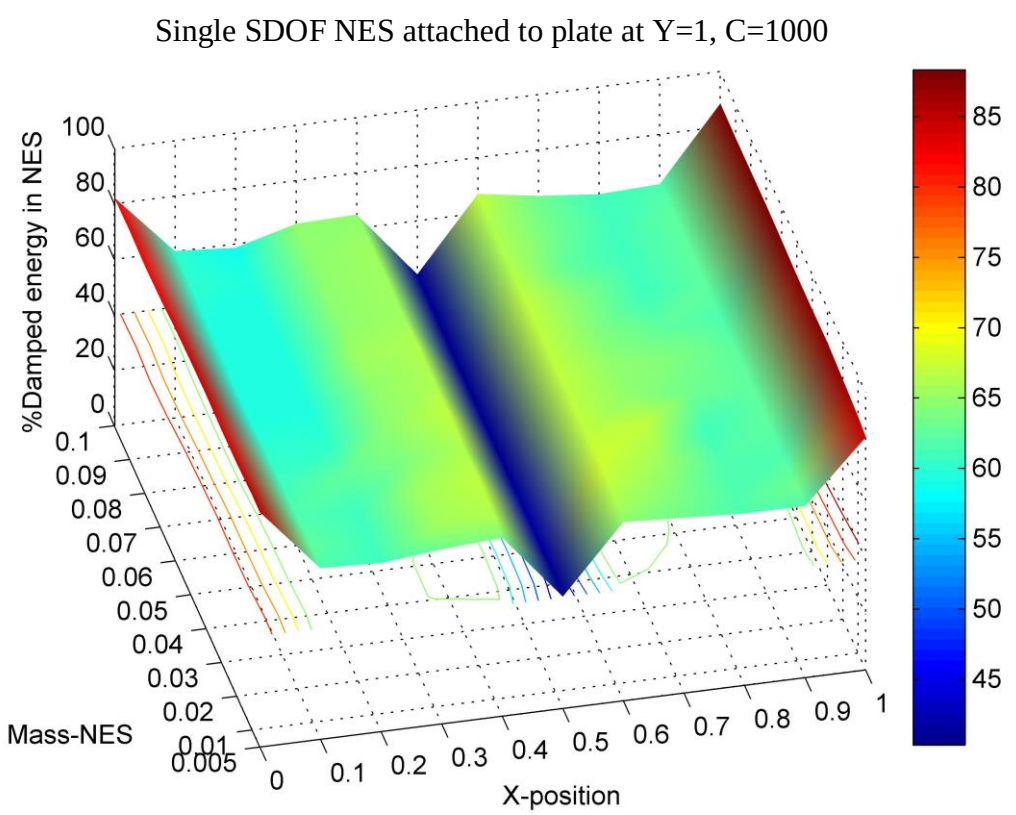

Figure 4a

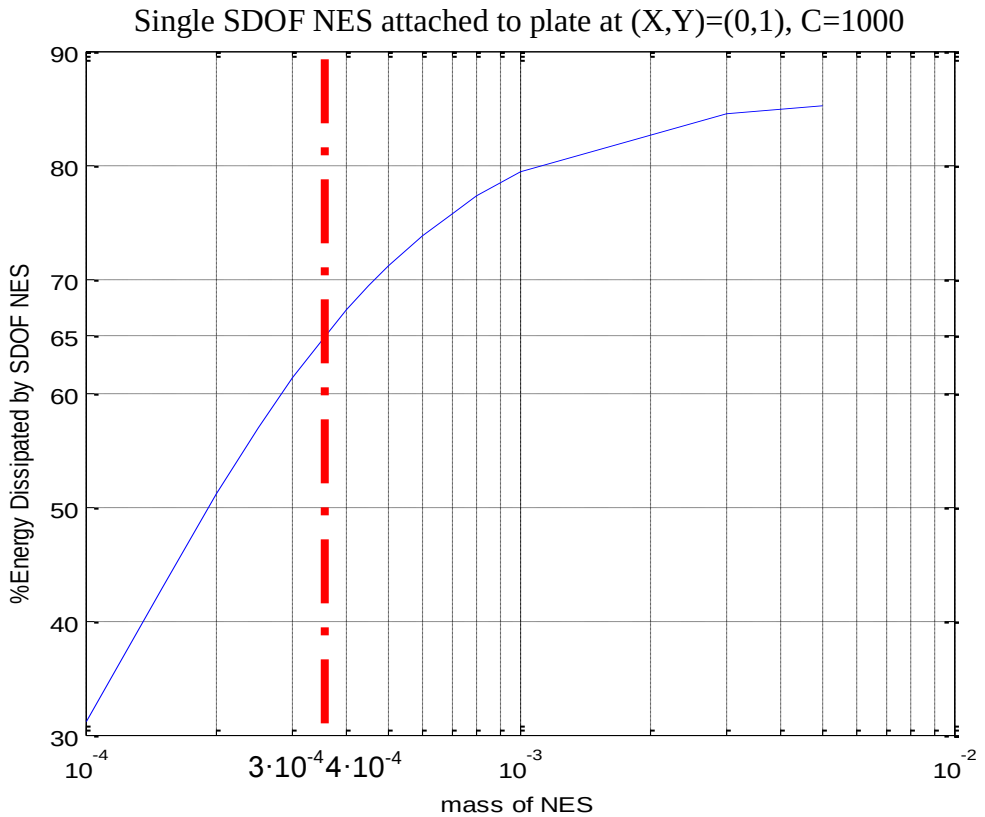

Figure 4b. Parametric study of TET efficiency, (a) as function of NES mass and x-position of the NES on the plate for fixed y = 1; and (b) as function of NES mass when the NES is located at the optimal position (x,y)=(0,1).

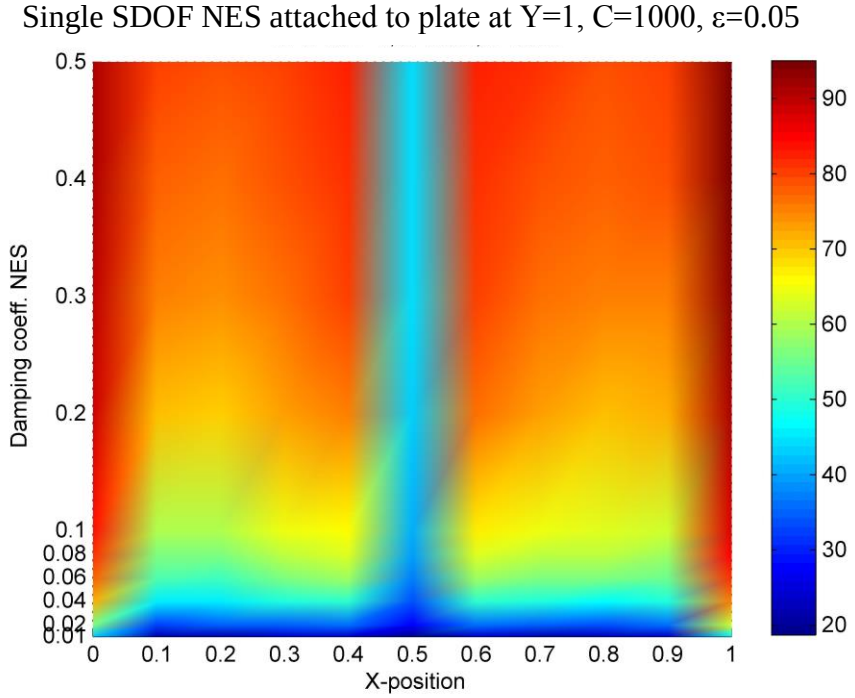

Figure 5. Parametric study of NES efficiency as function of its damping coefficient, and its x-position on the plate for fixed y = 1.

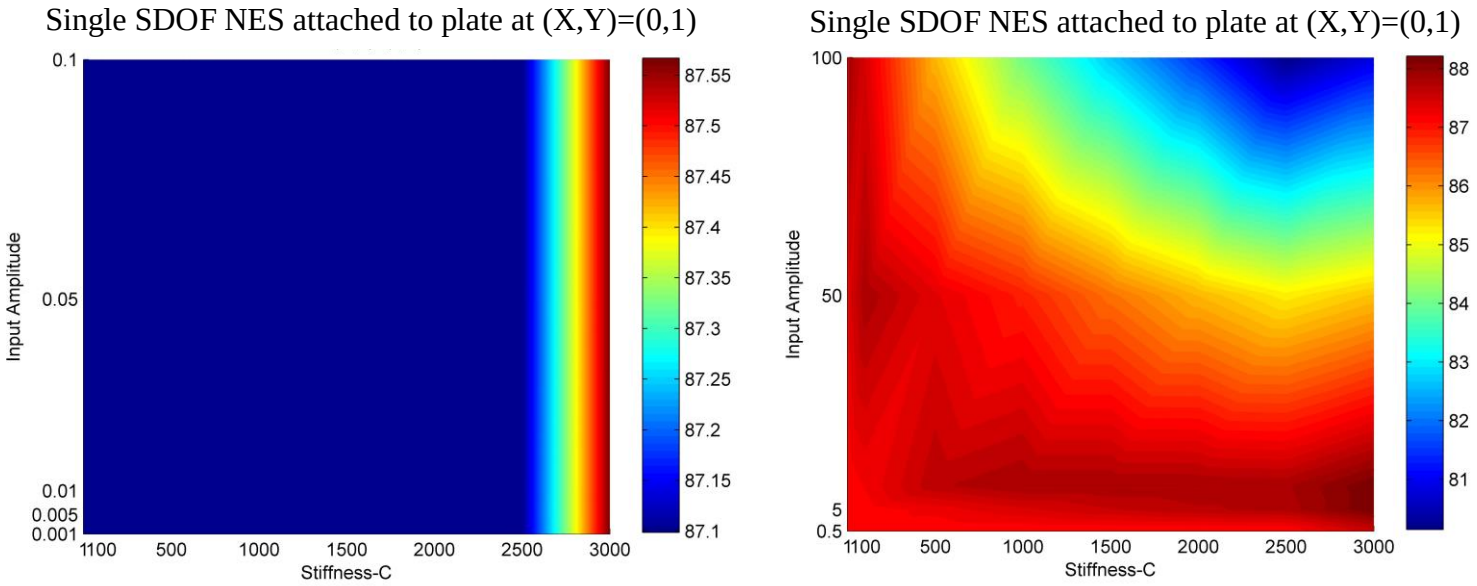

Figure 6. Parametric study of NES efficiency as function of the input amplitude (energy) and its stiffness C, at position (x,y)=(0,1).

In Figures 6a,b we depict the results of this parametric study. Note the weak dependence of TET efficiency on the input energy: indeed, TET efficiency for low input amplitudes and all values of C is of the order of 87%, but as the input amplitude and the nonlinear stiffness characteristic increase the TET efficiency decreases but within a very small range, less than 7%. Similar results have been reported by Georgiades et al. (2007) but without paying attention to restrict the examination of the energy dissipation within a range of input energy that it is of interest in engineering point of view.

A general conclusion from this first parametric study is that strong TETs can be realised from a plate with single or multiple shock excitation to a SDOF essentially nonlinear attachment, especially, when the NES is located at points of the plate corresponding to antinodes of energetically high plate modes. Indeed, it is possible to

passively transfer and locally dissipate at the NES as much as 87% of the shock energy of the plate. Moreover, the integrated plate-NES system can be designed so that TET efficiency is insignificantly affected by the magnitude of the applied shock within a specified range of design interest.

We now wish to study in more detail the nonlinear modal interactions that give rise to TET in the plate – SDOF NES system under consideration. To this end, we isolate a specific case corresponding to a plate with parameters given by (3), and an NES with nonlinear stiffness characteristic C = 1000, damping coefficient $\lambda = 0.1$, and mass, $\varepsilon = 0.05$. We assume that there is a single applied shock in the form of a half-sine (as defined in the previous section) at (x,y) = (1,1), e.g., at one of the free corners of the plate. Moreover, we assume that the SDOF NES is attached to the plate at position (x,y) = (0,0.5). In this specific case 64.35% of the shock energy of the plate gets eventually transferred to and locally dissipated by the NES. The sampling frequency for this simulation is 800 Hz that corresponds to Nyquist frequency 400 Hz (18 times more than the frequency of the 15^{th} linear mode that is 22.075 Hz) with total instantaneous energy varying between 99.86% and 100.01% of the applied shock energy.

We examine the transient nonlinear resonance interactions (transient resonance captures - TRCs) between the plate response at the point of attachment to the NES, and the NES response. We focus mainly in the early stage of the transient dynamics, where the energy of the system is at high levels and the nonlinear effects are expected to be more profound; hence, we examine TRCs in the early time interval $0 < t < 5$, during which more than 75% of the shock energy is been dissipated by the dampers of the integrated system. The responses of the plate and the NES are decomposed in terms of Intrinsic Mode Functions (IMFs) using Empirical Mode Decomposition (EMD) (Georgiades, 2006); these are oscillatory modes embedded in the respective time series. Then, we apply the Hilbert transform to each IMF to determine its instantaneous amplitude and frequency. By superimposing the instantaneous frequencies of the IMFs to the wavelet spectra of the corresponding responses we can determine the dominant IMFs as depicted in Figures 7a-e; this technique was first developed in (Georgiades et al., 2007). The determination of the dominant IMFs of the plate and NES responses enables us to detect the dominant TRCs that govern TET in this case.

Considering the plate response, the 5^{th} and 6^{th} IMF are dominant (cf. Figures 8a,b), whereas, the 1^{st}, 2^{nd} and 3^{rd} IMF of the NES response are dominant as well (cf. Figures 8c-e). By computing the ratios of the instantaneous frequencies of the dominant IMFs of the plate and the NES responses we can identify the possible types of $(k:m)$ TRCs that occur in the transient dynamics, as well as, the corresponding time intervals where these TRCs take place. Considering the instantaneous frequency plots depicted in Figure 8 we detect the following 1:1 TRCs between, (a) the 5^{th} IMF of the plate and the 3^{rd} IMF of the NES at frequency close to 1.9 Hz in the time interval $0.25 < t < 3.25$ (TRC I); (b) the 5^{th} IMF of the plate and the 1^{st} IMF of the NES close to 1.9 Hz in the time interval $6 < t < 12$ (TRC II); and, (c) the 6^{th} IMF of the plate and the 2^{nd} IMF of the NES close to 1.9 Hz in the time interval $8 < t < 14$ (TRC III). These TRCs are responsible for passive TET in the specific case under examination and the presented analysis helps to identify the corresponding nonlinear resonance interactions between the embedded oscillatory modes in the plate and NES responses.

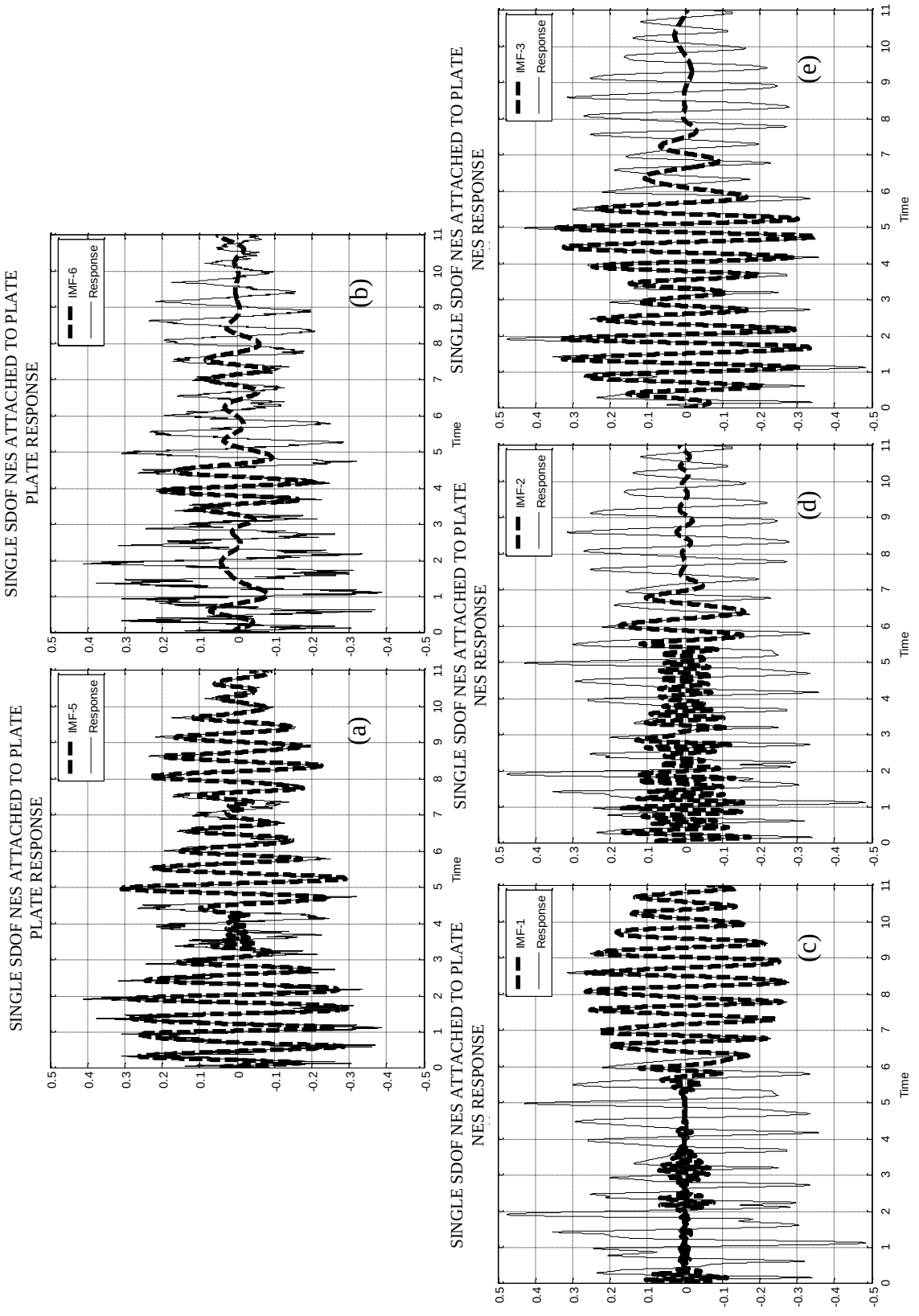

Figure 7. Dominant IMFs of the response of the SDOF NES, and of the plate response at the point of attachment to the NES, superimposed to the corresponding time series.

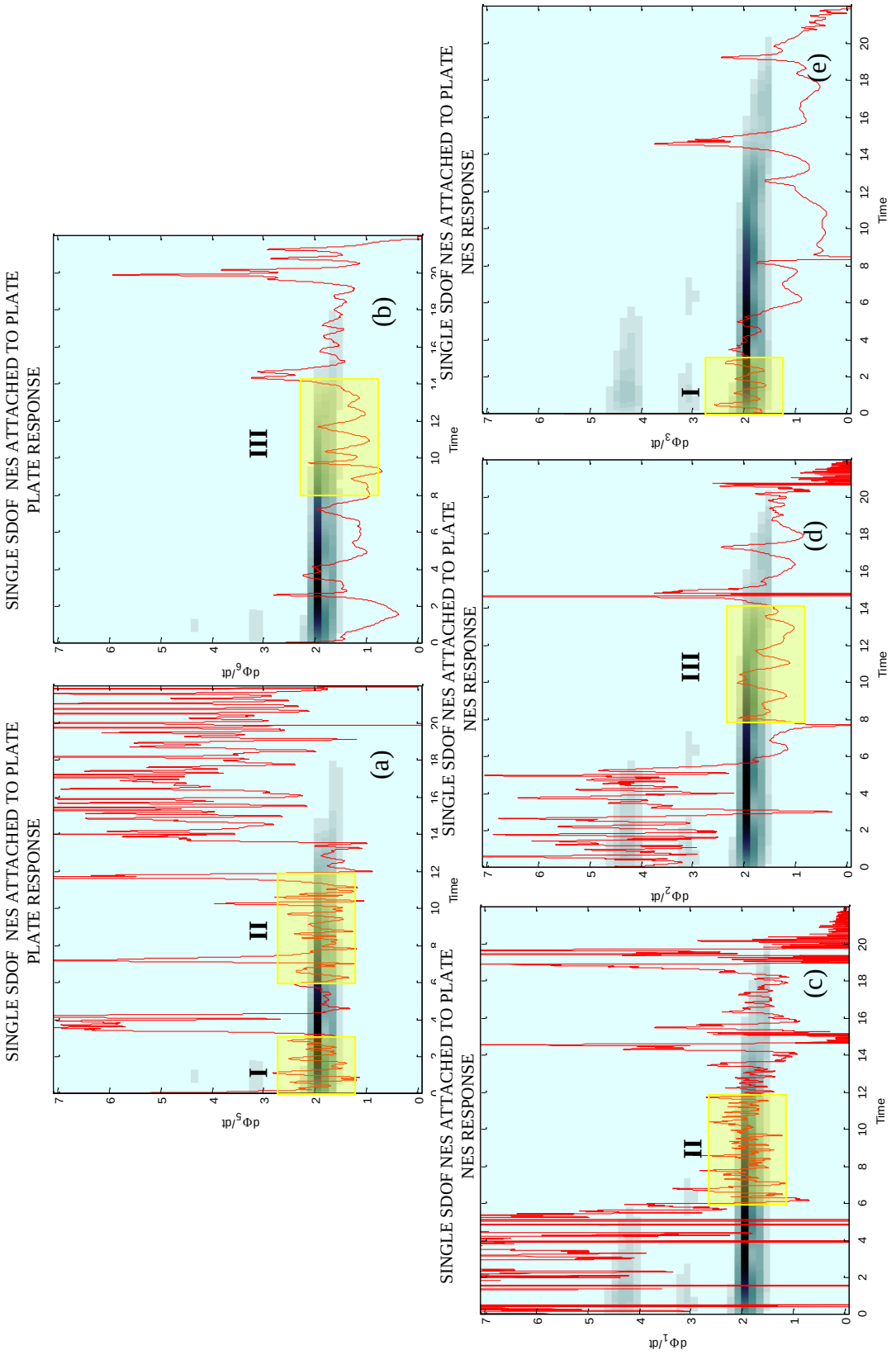

Figure 8. Instantaneous frequencies of the dominant IMFs superimposed to the corresponding Wavelet Transform spectra: (a,b) 6th and 7th IMF of the plate response, (c,d,e,f) 1st, 2nd, 3rd and 4th IMF of the SDOF NES response; dominant 1:1 TRCs between IMFs are indicated by I, II and III.

5. Parametric Studies of TET from the Plate to multiple SDOF NESs

The parametric study of TET efficiency in terms of NES location on the plate carried out in section 4 revealed locations where TET efficiency is low (when the NES is attached close to nodal curves of plate modes), and alternative locations where the TET efficiency is high (of the order of more than 70%). The computational study carried out in this section aims to examine enhancement of TET through the use of multiple SDOF NESs, model 3 with equations (1.1, 1.6-1.9). The parameters used for the plate and the input force in the following numerical simulations are identical to those employed in the simulations of section 4. Two SDOF NES are attached to the plate, with each possessing mass $\varepsilon = 0.005$ (e.g., 0.5% of the total mass of the plate), stiffness $C = 1000$, and damping coefficient $\lambda = 0.1$. A single shock excitation is applied to the plate, of the same form and position as in the previous section. For this set of simulations the sampling frequency used is 441.5 Hz that corresponds to Nyquist frequency of 220 Hz (10 times more than the frequency of the 15th linear mode that is 22.075 Hz), except for the final case which was carried out with a sampling frequency of 2208 Hz which corresponding to a Nyquist frequency of 1104 Hz (50 times more than the frequency of the 15th linear mode that is 22.075 Hz); the total instantaneous energy varied between 99.67% and 100.31% of the applied shock energy.

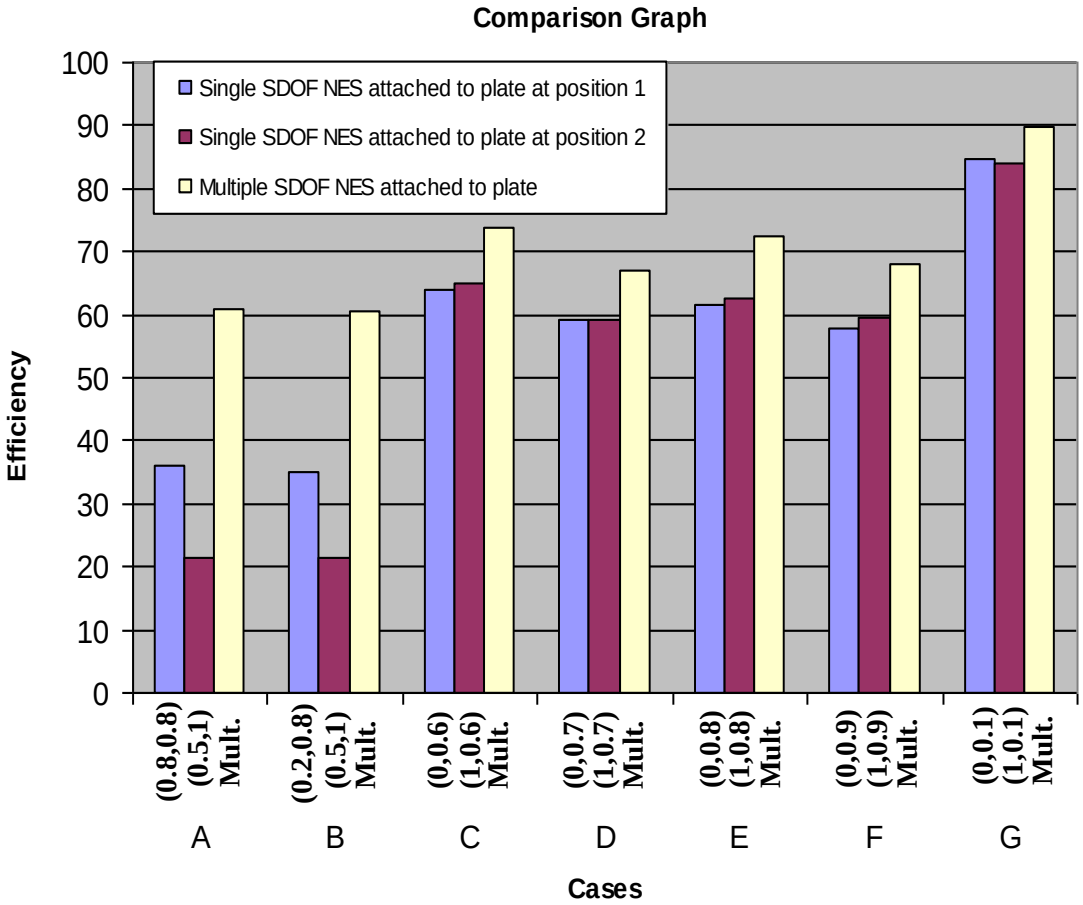

Figure 9. Comparative study of TET efficiency when using two single NESs, and a set of two NESs; single shock excitation of the plate.

In the numerical simulations that follow we examine seven specific cases (designated Cases A-G) where two NESs are located at various positions on the plate. Of specific interest are cases where the NESs are located at nodal curves of plate modes. In Figure 9 we depict a bar diagram depicting NES efficiencies for all seven cases considered; we compare the efficiencies of single NESs located in either one of the two locations occupied by that positions the set of NESs, to the efficiency of the set of two NESs when they are both attached to the plate at the same time. In each case we indicate the position of the two NESs. For case A the TET achieved when using single (isolated) NESs is 36.13% and 21.58%, respectively, whereas when using the combined set of two NESs at the same locations TET increases to 61.02%, e.g., it exceeds the sum of TETs when the two NESs are applied in isolation. This demonstrates a positive synergy effect of the set of two NESs, which, however, is not expected to persist in the other cases where NES locations more favourable to TET are considered.

In case B, the first NES is located at position (x,y) = (0.2,0.8) which is a crossing point of the nodal curves of the 3rd and 4th plate modes, and the second NES at (x,y) = (0.5,1), e.g., the location that led to the lowest TET efficiency when a single NES was used. Again, in this case the efficiency of the set of two NESs increases significantly to 60.4% (cf. Fig. 9), which again exceeds the summation of the individual NES efficiencies when applied in isolation at the same locations. Again, this demonstrates positive synergy of the set of two NESs. Hence, it appears that the minimum level of TET that one achieves when using a set of two SDOF NES exceeds 60%, which represents an improvement compared to the case when a single NES is used; this result is further enhanced by the positive synergy achieved when the pair of NESs is used.

In cases C, D, E and F we located the set of NESs at different positions of the plate to investigate the synergistic TET efficiency when the NESs are located at regions of high individual TET efficiency for the SDOF NES (between 60-70% - such locations are at the edges of the plate at x = 0 and x = 1). For cases C, D, E and F we place the NESs at the edges of the plate, x = 0, 1, with y = 0.6, 0.7, 0.8 and 0.9, respectively. For these cases we note a slight improvement (about 10%) of the synergistic efficiency of the set of two NESs (cf. Fig. 9).

Finally, there are two locations where the efficiency of the single SDOF NES is very high (more than 80%); these are the two free corners of the plate. The numerical simulations indicate that by attaching the set of two NESs at these locations (case G), we obtain a combined TET efficiency of 89.9%, which can be considered as the optimal synergistic TET efficiency that can be achieved by the set of two NESs on the plate. We note, however, that the improvement in TET efficiency compared to using the two NESs in isolation at the same locations is only marginal.

A general conclusion drawn from the mentioned simulations is that the use of the set of two NESs improves TET efficiency in regions where the use of single (isolated) NESs leads to poor TET performance. In such regions there occur positive synergisms between the two NESs of the set, which leads to TET efficiencies that exceed the sum of the efficiencies of single NESs when these are used in isolation. The use of multiple NESs, however, improves only marginally TET efficiency in locations where the isolated NESs already provide good TET performance.

6. Parametric Studies of TET from the Plate to a single MDOF NES

We now consider TET from the plate to a single MDOF NES. The equations of motion of this system are given by model 4 with equations (1.1, 1.10-1.14), and the TET efficiency is judged by the energy dissipation measures (13) and (14) and their long-time asymptotic values. The first set of numerical

simulations of this series was performed in order to examine the influence of the linear coupling stiffness between the plate and the MDOF NES to TET efficiency. The parameters used for the plate are identical to the ones used for the case of SDOF NES attachment, relations (3), and the applied shock is identical to the half-sine excitation used in previous simulations, relation (4); the duration of the applied shock was selected sufficiently small to directly excite at least the leading five modes of the plate – however, as mentioned in previous Sections additional plate modes may be indirectly excited by nonlinear coupling provided by the MDOF NES. The three masses of the MDOF NES are assumed to be small, $m_1 = m_2 = m_3 = 0.0017$ (≈0.005/3), e.g., the total mass of the MDOF NES is assumed to be identical to the smallest mass of the SDOF NES used in the parametric study of section 4. In this way we wish to study the relative advantage of replacing the SDOF NES by a MDOF one, *without burdening the plate with additional mass*. The two nonlinear stiffnesses of the NES are selected as, $C_1 = 5$, and $C_2 = 0.1$, whereas the two dampers of the NES possess the same coefficient, $\lambda=0.1$. For this set of simulations the sampling frequency used is 800 Hz that corresponds to Nyquist frequency of 400 Hz (18 times more than the frequency of the 15th linear mode that is 22.075 Hz), with total instantaneous energy varying between 100.0% and 100.90% of the applied shock energy.

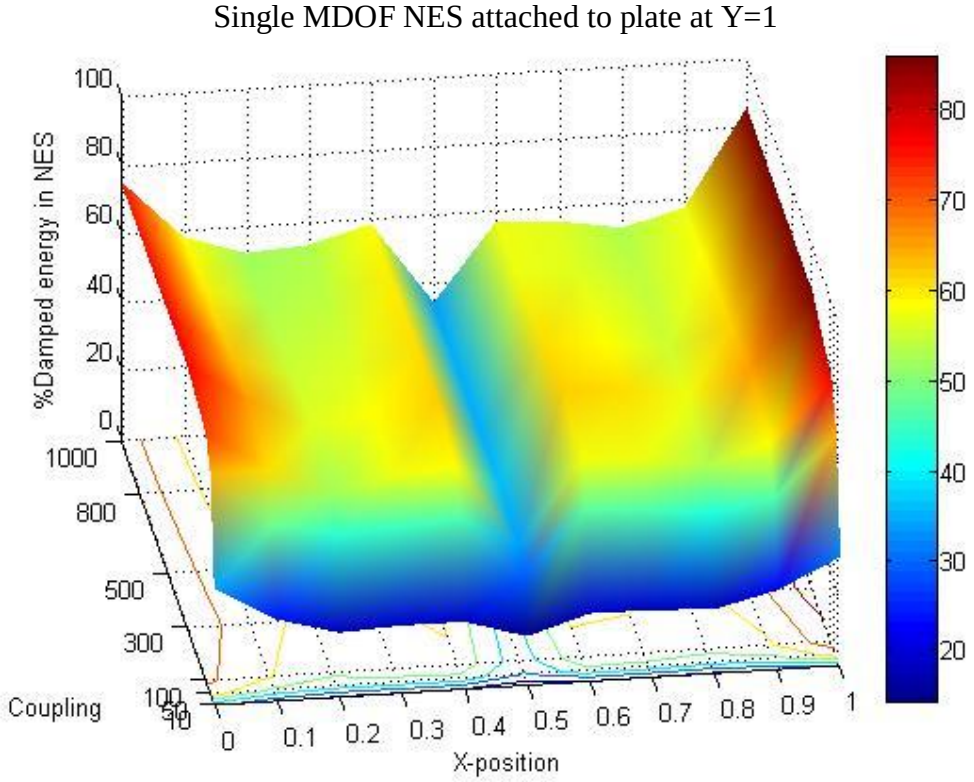

Figure 10. Parametric study of TET efficiency as function of the (linear) coupling stiffness C_0 of a MDOF NES and its x-position, for fixed y = 1.

In Figure 10 we depict the long-time asymptotic value $\eta_{1t>>1} + \eta_{2t>>1} = \lim_{t>>1}\left[\eta_1(t) + \eta_2(t)\right]$ (which represents the portion of shock energy of the plate that is eventually dissipated by the two dampers of the MDOF NES) as function of the coupling stiffness C_0 ($C_0 \in [10,1000]$), and the x-position of the NES for the representative 'y-slice' y=1. A first conclusion from these numerical results is

that TET efficiency appears to be robust as C_0 varies above the threshold of C_0=100, for every x-location of the NES (as depicted in Figure 10). Moreover, strong (efficient) TET from the plate to the MDOF NES is realized for relatively stiff coupling stiffness. Maximum TET efficiency of the MDOF NES reaches levels of 80%, which are comparable to maximum TET efficiency achieved by SDOF NESs. Similarly to the case of the SDOF NES, the variation of the position of the MDOF NES appears to strongly affect TET from the plate to the NES, as depicted in Figure 10; however, this will be more evident in the second set of simulations that we now proceed to discuss.

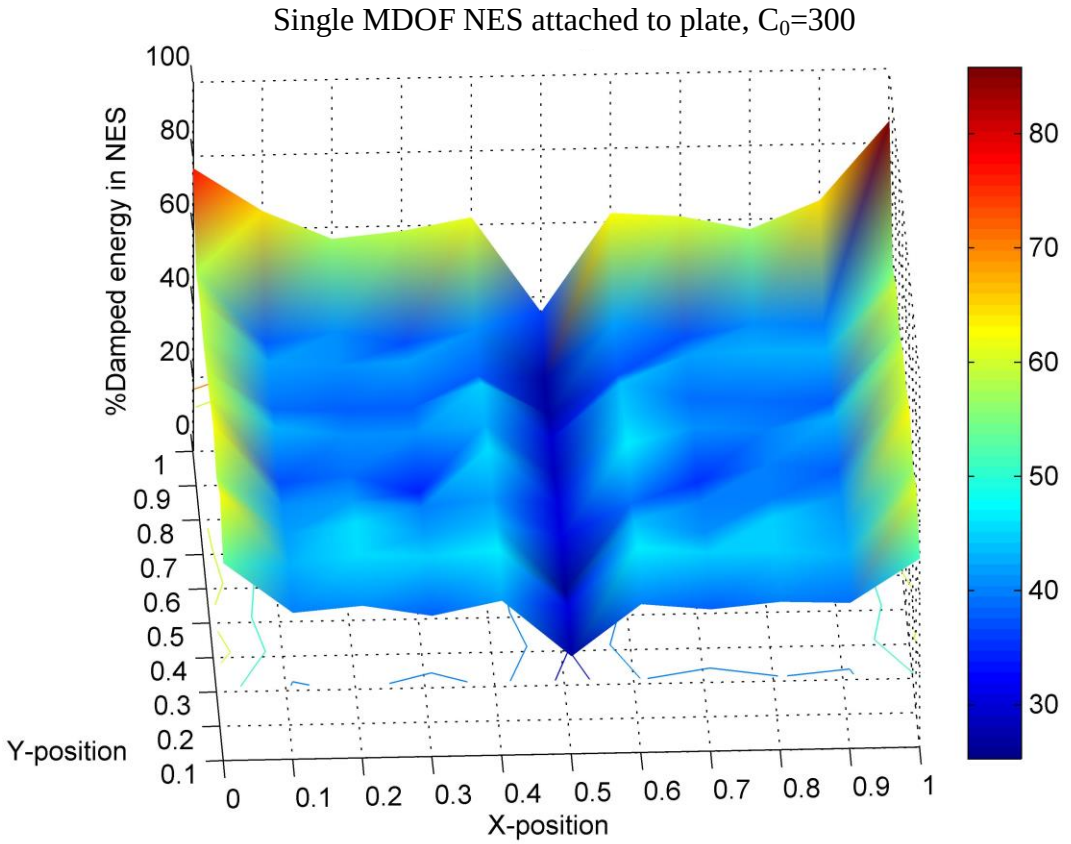

Figure 11. Parametric study of TET efficiency for a MDOF NES located at every possible position on the plate, for coupling stiffness $C_0 = 300$.

In the second set of simulations we examine the influence of the MDOF NES position on TET; for this, we examine MDOF NES placement at every possible position on the plate (with a mesh of 10×10 elements), not restricting our study to any specific 'y-slices.' We use the same set of NES parameter values with the previous set of simulations, and fix the coupling stiffness to C_0=300. For this set of simulations the sampling frequency used is 800 Hz that corresponds to Nyquist frequency of 400 Hz (18 times more than the frequency of the 15th linear mode that is 22.075 Hz), with total instantaneous energy varying between 100.0% and 100.90% of the applied shock energy.

In Figure 11 we depict TET efficiency for the NES located at every possible position on the plate. Predictably, the highest values of efficiency of the MDOF NES are obtained at the free corners of the plate, reaching 85.85% when the NES is located at (x,y) = (1,1), and 76.67% when located at (x,y) = (0,1); as explained in previous Sections, at these positions the MDOF NES can interact with all plate modes, as no nodal curves of low order plate modes are located nearby and the plate posses the maximum displacement. Similarly to the case of SDOF NES, the interpretation of the results depicted in Figure 11 should be

carried out in conjunction with Table 1, which depicts the nodal curves of the first five modes of the linear, uncoupled plate with no dispersion (the 'plate modes'). Moreover, the efficiency of the NES decreases when the NES is located closer to the clamped end, where the displacements of the plate are small and the nonlinear effects are less profound. Since passive TET is the result of nonlinear resonance interactions (resonance captures) between the plate and the NES it is reasonable to expect that in low-amplitude regimes the effectiveness of the MDOF should deteriorate. As demonstrated, however, in (Tsakirtzis et al., 2007) it is possible (under certain forcing conditions and at definite ranges of NES parameters) to achieve efficient TET from a directly forced linear system to a MDOF NES, even at low amplitude regimes; such a case, however, was not realized in the simulations considered herein.

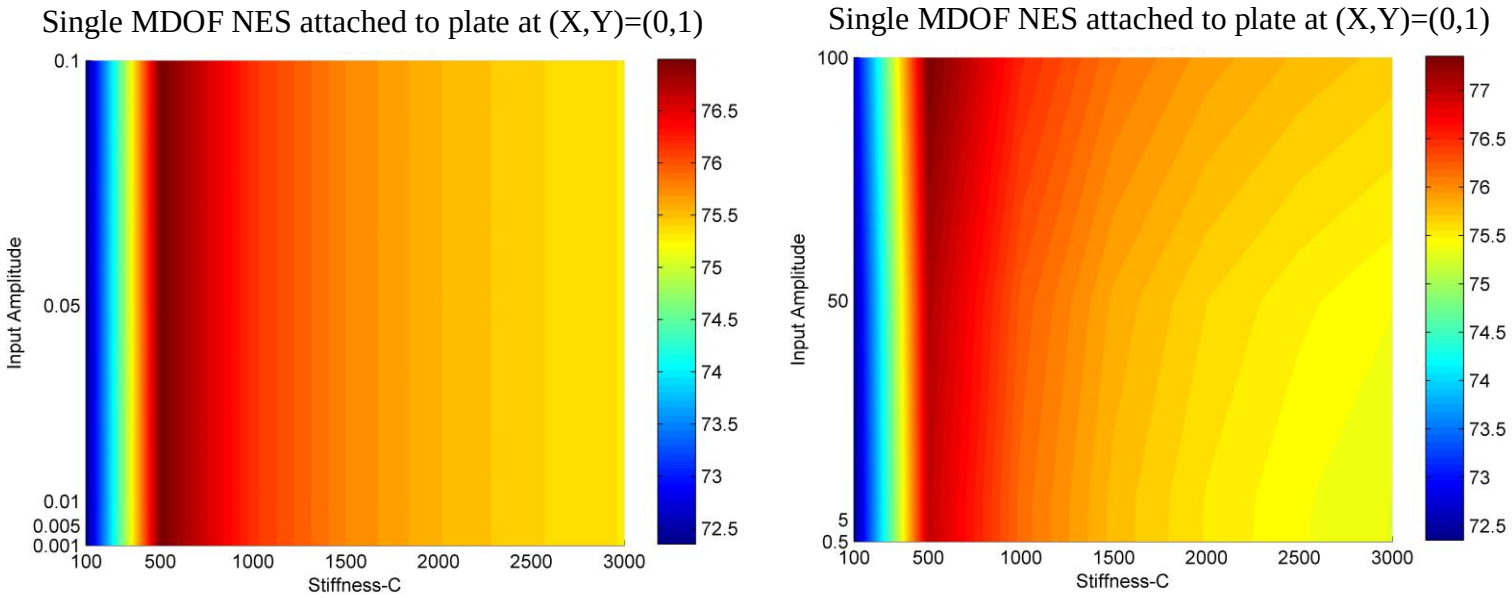

Figure 12. Parametric study of MDOF NES efficiency as function of the shock amplitude (energy) and coupling stiffness C_0.

The third set of numerical simulations of this series was performed in order to examine the influence of the magnitude of the applied shock and the (linear) coupling stiffness C_0 to TET efficiency. The parameters of the system used for this set of simulations are identical to the first set of simulations reported in this section, for varying shock amplitude in the range $A \in [0.001,100]$. For the third set of simulations the sampling frequency used is 800 Hz that corresponds to Nyquist frequency of 400 Hz (18 times more than the frequency of the 15th linear mode that is 22.075 Hz) with total instantaneous energy varying between 100.0% and 102.3% of the applied shock energy.

In Figures 12a,b we depict the results of this parametric study. We note that TET efficiency does not depend significantly on the variation of shock input; indeed, the variation of TET efficiency for the range of shocks examined is less than 6%, lying within the range 72-77.5%. Additionally, TET efficiency is uniformly more than 72% in these simulations, which assures satisfactory NES performance in the entire range of parameters considered.

The fourth set of numerical simulations of this series was performed in order to examine the optimum values of the other stiffness parameters C_1,C_2 when the NES is located at the free corner (x,y)=(0,1) of the plate (highest efficiency away from the excitation point) with the optimum coupling stiffness C_0=300. The parameters of the

plate and damping coefficients were identical to the other sets of simulations of this section. For the fourth set of simulations the sampling frequency used was 1000 Hz that corresponds to Nyquist frequency of 500 Hz (45 times more than the frequency of the 15th linear mode that is 22.075 Hz), with total instantaneous energy varying between 100.0% and 101.70% of the applied shock energy. The results for this set of simulations are depicted in Figure 13. We note that strong TET is realized over a broad range of values of C_1,C_2, with optimal stiffness values being realized for $C_1 \approx 3000$ and $C_2 \approx 10$. We note that increasing the value of the nonlinear stiffness coefficients does not necessarily result in TET enhancement; this is due to the fact that very stiff nonlinear connections in the MDOF preclude the realization of large relative motions between the masses of the NES, and as a result to smaller amounts of energy dissipated by its dampers. Moreover, we note that optimal TET occurs in highly asymmetric MDOF NES configurations, a result that agrees with the findings of a previous work on discrete oscillators with MDOF NESs attached (Tsakirtzis et al., 2007). This is due to the fact that in such highly asymmetric MDOF NESs, a part of the NES (the one in closer proximity to the plate corresponding to the stiffer stiffness C_1) acts as broadband resonator that engages modes of the plate in transient resonance captures (TRCs), whereas the complement of the NES (the one further away from the plate corresponding to the weaker stiffness C_2) acts as dissipater of shock energy.

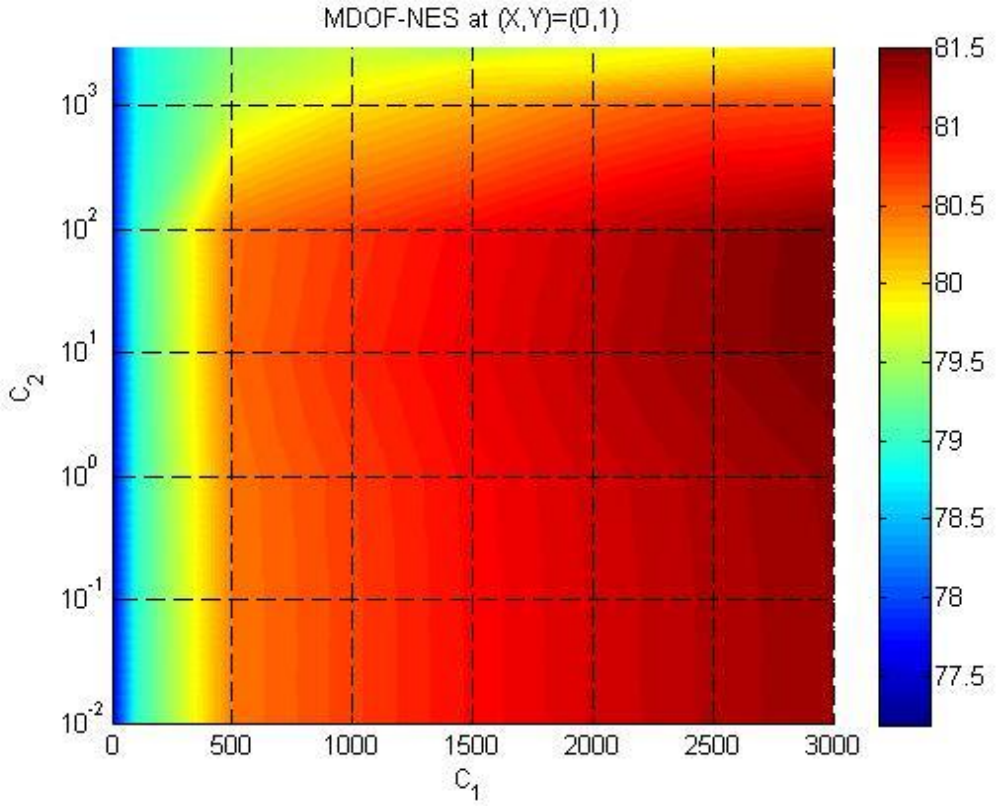

Figure 13. Parametric study of MDOF NES efficiency as function of nonlinear stiffness C_1 and C_2.

The analysis of the complex nonlinear modal interactions and of the corresponding transient resonance captures that govern TET in this system can be performed by applying the previous combined Wavelet/EMD postprocessing methodology. As the analysis becomes quite involved (since there the transient responses of three different masses of the NES that must be considered in this case), the reader is referred to (Georgiades, 2006) for a detailed presentation of the results of this analysis for specific cases. In the next section we consider the

alternative of using a linear vibration absorber in order to demonstrate the qualitative differences of the proposed essentially nonlinear designs.

7. The Linear Alternative: Tuned Mass Damper (TMD) – Comparative Study

In this section we present the results of a parametric study of the plate with a linear Tuned Mass Damper (TMD) attached, model 5 with equations (1.1, 1.15-1.17). We assess the capacity of the TMD to absorb and locally dissipate shock energy from the plate, by varying the TMD parameters and its position on the plate. We perform a series of simulations considering single and multiple shock excitations applied to the plate. In each of these sets, the efficiency of the TMD to passively absorb and locally dissipate shock energy from the plate is estimated by the following limit,

$$\eta_{t>>1} = \lim_{t>>1} \eta(t), \quad \eta(t) \equiv \frac{E_{damp,NES}(t)}{E_{in}} = \frac{\lambda \int_0^t \left[\dot{w}(d_x, d_y, \tau) - \dot{v}(\tau) \right]^2 d\tau}{\int_0^t F(\tau)\, \dot{w}(b_x, b_y, \tau) d\tau} \qquad (15)$$

where $v(t)$ is the response of the TMD. This represents the portion of the shock energy of the plate that is eventually dissipated by the damper of the TMD, and is similar to the energy measures defined previously to assess the efficiency of SDOF and MDOF NESs.

In the first set of simulations we examine the efficiency of the TMD to absorb and dissipate shock energy by varying its stiffness and its location on the plate, for single shock excitation [as defined by (4)]. The system parameters of the plate properties are defined in (3), the TMD mass is $\varepsilon = 0.05$, and its damping coefficient is $\lambda = 0.1$; these were identical to the parameters used for the simulations with the SDOF NES attachment (section 4), so the two sets of simulations can be directly compared. For this set of simulations the sampling frequency used is 600 Hz that corresponds to Nyquist frequency of 300 Hz (13 times more than the frequency of the 15^{th} linear mode that is 22.075 Hz), with total instantaneous energy being conserved (within an error of less than 0.001% of the applied shock) when energy dissipated by the dampers of the system is taken into account.

In Figure 14 we depict the efficiency of the TMD depending on its stiffness and on its x-position on the plate for the fixed 'y-slice' y = 1 (e.g., at the free end of the cantilever plate). This result should be compared to the plot of Figure 2a for the SDOF NES. We note that the variation of the location of the TMD strongly affects its efficiency, in a similar manner to the SDOF and MDOF NES attachments examined previously. Indeed, when the TMD is located at positions close to nodal lines of the plate, the TMD can not interact with the corresponding plate modes, and therefore the absorption of shock energy from the plate deteriorates. Moreover, when the TMD is 'tuned' to the i-th plate mode, e.g., when its stiffness is equal to $k_{ln} = \omega_i^2 \varepsilon$ (undamped case), where ω_i is the i-th natural frequency of the (uncoupled and linear) plate, its efficiency in extracting energy from that mode is high. It must be noted that the difference in the efficiency between the two extreme corners (x=0, and x=1) in the attached potions (left part and right part of Figure 13) is due to the fact that the excitation force is on the right corner (x=1) and therefore there is an effect that the TMD is absorbing energy from the excitation force directly. However, for relatively high stiffness values of the TMD, e.g., when it is 'detuned' from the leading plate modes, its efficiency deteriorates; this result is in agreement with similar results reported in the literature (Frahm 1911, Den Hartog 1947). Comparing to plot of Figure 2a we note that the efficiency of the SDOF NES does not show such dependence on stiffness, and hence, its performance is more robust to stiffness variations.

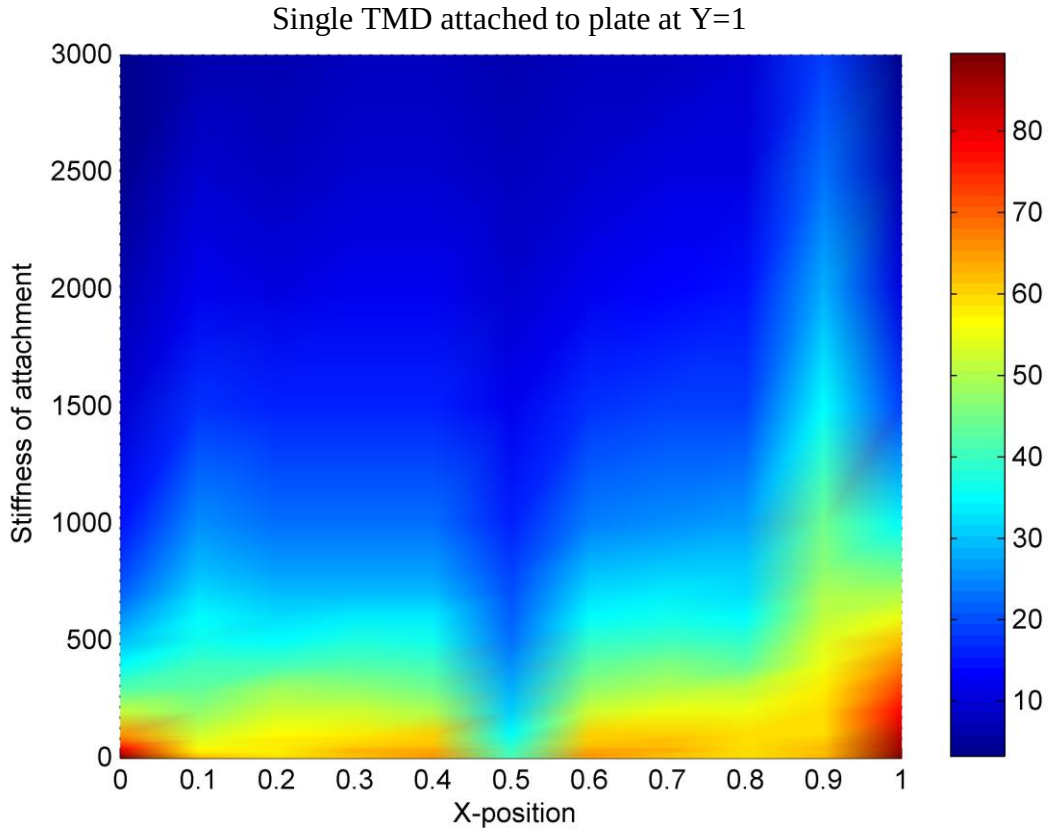

Figure 14. Efficiency of the linear vibration absorber-TMD as function of its stiffness and its x-position on the plate for the 'y-slice' y = 1, single shock excitation.

In the second set of simulations we examine the efficiency of the TMD for variation of its stiffness and location of the TMD for multiple shock excitations. The parameters used are identical to the first set of simulations, but the damping coefficient of the plate was selected as, d = 15, and the TMD mass as, ε = 0.005; these system parameters are identical to the ones used in section 5, where the efficiency of the SDOF NES for multiple shock excitations was examined. For the second set of simulations the sampling frequency used is 164.6 Hz that corresponds to Nyquist frequency of 82.3 Hz (3.5 times more than the frequency of the 15th linear mode that is 22.075 Hz) and again the total energy of the system being conserved for the entire durations of the simulations when dissipative terms are included.

In Figure 15 we present the results for this set of simulations. Again, the stiffness and position of the TMD strongly affect its efficiency. Comparing these results to the plot of Figure 2b we again note the insensitivity of the performance of the SDOF NES to stiffness variations for multiple shock excitation.

In the third set of simulations we examine the effect of varying the TMD mass on its energy absorption efficiency. Single shock excitation is considered for this set of simulations. For this set of simulations the sampling frequency used is 300 Hz that corresponds to Nyquist frequency of 150 Hz (6 times more than the frequency of the 15th linear mode that is 22.075 Hz).

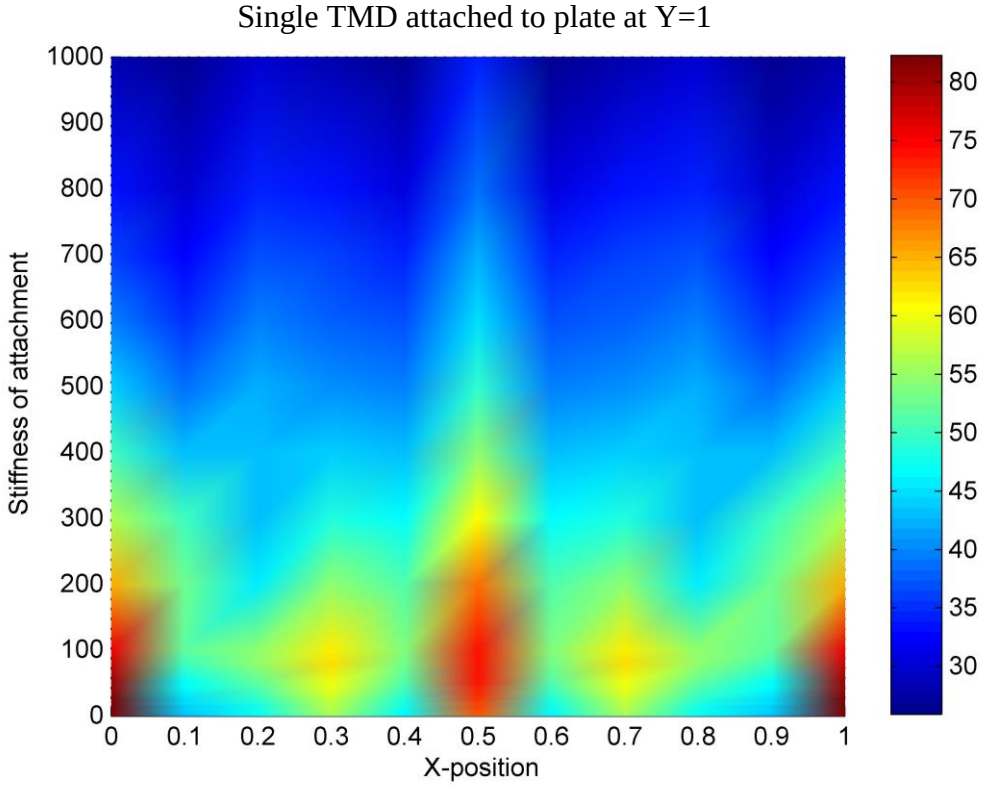

Figure 15. Efficiency of the linear vibration absorber-TMD as function of its stiffness and its x-position on the plate for the 'y-slice' y = 1, multiple shock excitations.

In similarly to the case of SDOF NES we aim to identify the threshold of mass value of the TMD above which the TMD is capable of absorbing at least 65 % of the shock energy of the plate. This threshold was computed to $\varepsilon = 0.0004$, e.g., slightly higher than the case of the SDOF NES attachment (cf. Figure 4b).

In order to compare the performance of the various nonlinear and linear attachment configurations considered in this work, we performed an additional set of simulations for fixed attachment placement at (x,y) = (0,1) on the plate, and away from the source of the (single) input shock at (b_x, b_y) = (1,1)]. For this set of simulations the plate parameters are defined in (3). All SDOF attachments considered possess mass equal to $\varepsilon = 0.005$ (or 0.005% of the plate mass), and viscous damper coefficients equal to λ = 0.1. For the simulations with SDOF attachment the sampling frequency used is 1766 Hz that corresponds to Nyquist frequency of 883 Hz (80 times more than the frequency of the 15th linear mode that is 22.075 Hz) and the minimum and maximum values of the % instantaneous total energy all over the simulations are 99.93% and 100.02% correspondingly, therefore the error is less than 0.1% in the determined values of energy.

For the MDOF NES each mass was chosen equal to 0.005/3, and the two viscous damping coefficients where selected as λ = 0.1; for simulations where the coupling stiffness (C_0) varies the two nonlinear stiffness coefficients are C_1 = 3000 and C_2 = 15; when the stiffness C_1 varies the other stiffness coefficients are C_0 = 300 and C_2 = 15; whereas, when C_2 varies stiffness the other stiffness coefficients are C_0=300 and C_1=3000. For the simulations with MDOF attachment the sampling frequency used is 1000 Hz that corresponds to Nyquist frequency of 500 Hz (45 times more than the frequency of the 15th linear mode that is 22.075 Hz); the total instantaneous energy varies between 100.0% and 101.75% of the applied shock energy.

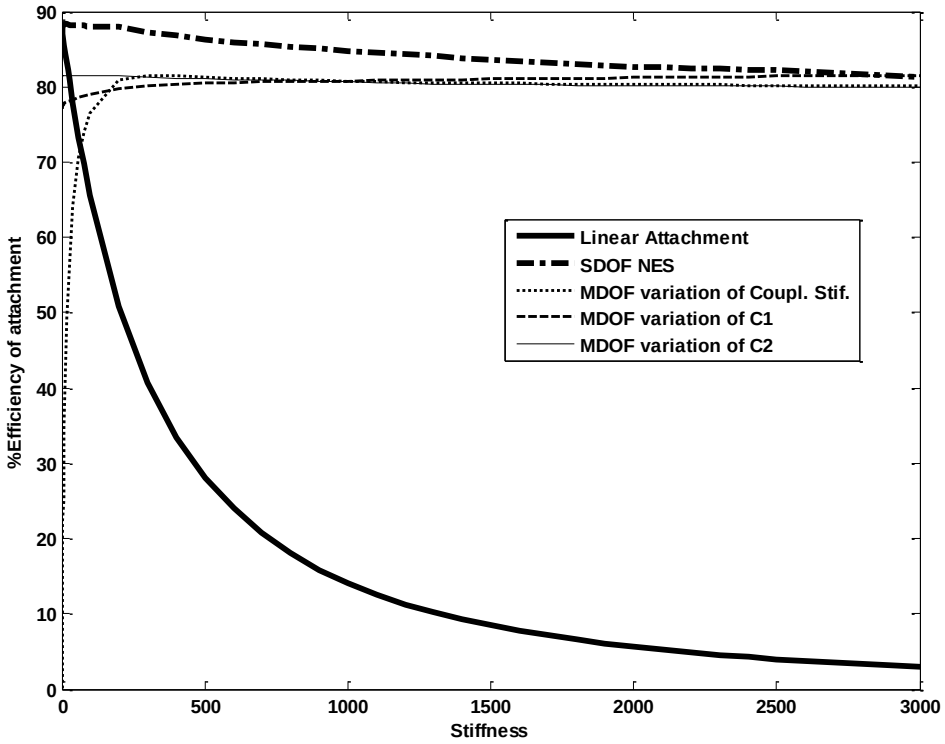

Figure 16. Comparison of TET efficiency of the different nonlinear and linear attachment considered in this work for varying coupling stiffness.

In Figure 16 we depict the results of this set of simulations, from which we deduce that the highest TET efficiency and robustness is achieved for the case of SDOF NES. As expected, the TMD is effective only when is 'tuned' to energetically strong plate modes, and its performance rapidly deteriorates when 'detuning' occurs. In contract, the essentially nonlinear SDOF and MDOF NESs possess no such detuning limitations as they lack a preferential 'tuning' frequency; hence, they are capable of engaging in transient resonance (resonance capture) with plate modes at arbitrary frequency ranges, with the only controlling parameter determining the resulting sequence of resonance captures being their instantaneous energies which 'tune' accordingly their instantaneous frequencies. The sequence of resonance captures that govern TETs can be studied in detail with the post processing methodology outlined in section 4.

Finally, we examine the performances of optimal configurations of the SDOF NES and the TMD, in order to compare their corresponding rates of targeted energy transfer for single forcing and for multiple forcing. In case of single forcing there is not significant difference but for multiple shock excitations as shown in Figure 17 there is significant difference. The plate parameters are given by (3) and distributed damping coefficient d = 15, with the attachments located at one of the free corners of the plate, (x,y) = (0,1), and their parameters given by, $\varepsilon = 0.005$, $\lambda = 0.1$, C = 100 for the SDOF NES, and $k_{ln} = 4.196$ for the TMD (e.g., tuned to the 4^{th} natural frequency of the uncoupled linear plate) and moreover for the TMD with $k_{ln} = 0.5142$ (e.g., tuned to the 1^{st} natural frequency of the uncoupled linear plate).

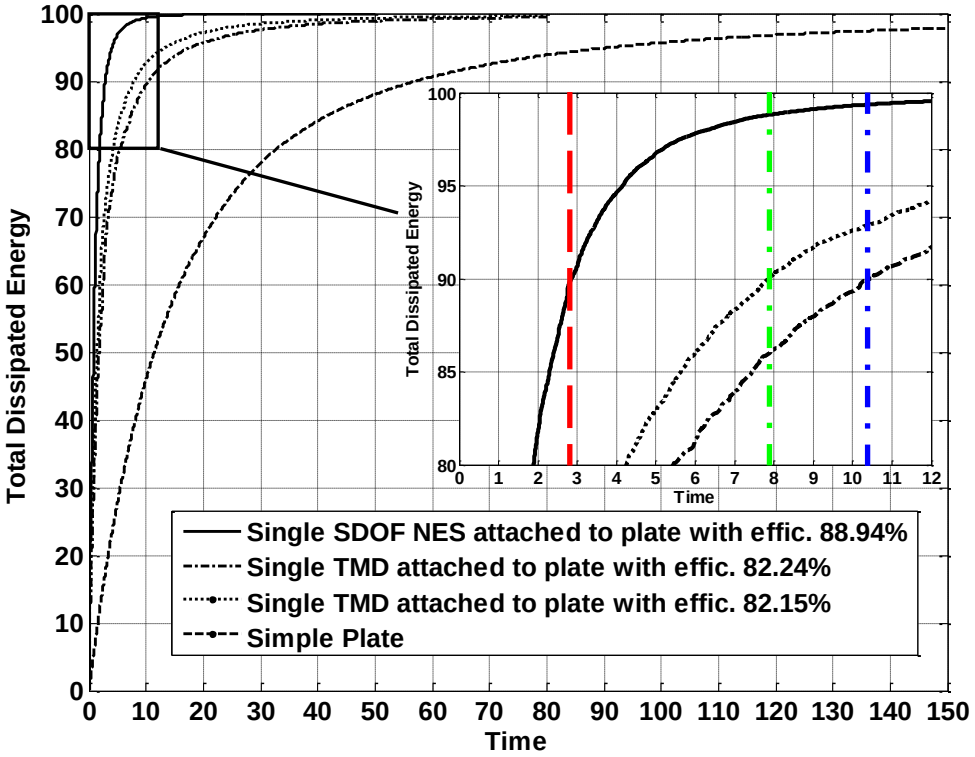

Figure 17. Time history of the total energy dissipated for single shock excitation for a plate with no attachments, and the same plate when a SDOF NES or a linear vibration absorber are attached.

For the specific optimal configurations considered, the corresponding TET efficiencies are 88.94% for the SDOF NES, and 82.24% and 82.14 for the TMD correspondingly to $k_{ln} = 4.196$ and $k_{ln} = 0.5142$.

. For the simulations with SDOF attachment the sampling frequency used is 1766 Hz that corresponds to Nyquist frequency of 883 Hz (80 times more than the frequency of the 15th linear mode that is 22.075 Hz), with total instantaneous energy varying between 99.93% and 100.02% of the applied shock energy. For the simulations with TMD attachment and the single plate the sampling frequency used is 800 Hz that corresponds to Nyquist frequency of 400 Hz (18 times more than the frequency of the 15th linear mode that is 22.075 Hz), and conserved total energy of the system (when dissipated energy is taken into account) at each time step of the simulations. Although the portions of shock energy eventually dissipated by these two configurations are comparable, the rates of TET for these two configurations differ drastically. The rates of shock energy dissipation can be deduced from the plots of Figure 17, where the total energy dissipation measure $\eta_{total}(t)$ is depicted as function of time; for comparison purposes the rate of energy dissipation in the uncoupled plate (e.g., the plate with no attachment where $\eta_{total}(t) = \eta_{plate}(t)$) is also depicted. We note that for multi-shock excitation the required time for the integrated plate – TMD system to dissipate 90% of the applied shock energy is approximately $t \approx 8$ and $t \approx 10.5$, whereas the corresponding time for the integrated plate – SDOF NES system is less than $t = 3$. Hence, nonlinear dissipation of shock energy occurs at a faster time scale, a result which is in agreement with the findings of previous works; actually, as shown in the Thesis by Georgiades (2006), the rate of nonlinear energy dissipation can be further increased by employing NESs with non-smooth stiffness characteristics, a feature which has already been explored in seismic mitigation designs (Nucera et al., 2007). In conclusion, apart from the lack of robustness of the

TMD for changes of parameters compared to the NESs (as depicted in Figure 16), the rate of shock energy absorption and dissipation in the linear design is smaller compared to the nonlinear design.

8. Concluding Remarks

We examined targeted energy transfers (TETs) from a shock-excited plate on an elastic foundation to nonlinear and linear attachments of alternative configurations: single SDOF NESs, multiple SDOF NESs, single MDOF NESs and single Tuned Mass Dampers (TDMs). In all cases examined the NESs considered were lightweight and possessed essentially nonlinear stiffnesses in parallel to linear viscous dampers. It was shown that the essential nonlinearities enable broadband TETs, e.g., sequences of transient resonance captures (TRCs) of the NESs with multiple modes of the plate over wide frequency ranges; moreover, for appropriate design of the NES parameters, the NES dampers were capable of dissipating the passively absorbed shock energy at sufficiently rapid pace, before this energy could backscatter to the plate.

The parametric study of the transient nonlinear dynamics of the SDOF NES attached to the plate demonstrated that the capacity of the NES to dissipate a significant portion of shock energy was robust to variations of NES stiffness, for both kinds of shock excitations, in the range of study ($O(10^2)$ - $O(10^3)$), and that there was a strong dependency of TET efficiency on the location of the NES on the plate. In fact, the highest values of NES efficiency (as judged by its capacity to passively absorb and dissipate a significant portion of the shock energy of the plate) were realized when the NES was placed at the free corners of the plate (where the plate response is maximum and away from nodal lines of the excited modes), whereas, it was significantly reduced when the NES was attached at locations close to the clamped end of the cantilever plate, or close to nodal lines of the plate modes. This is explained by noting that nonlinear effects (and, hence, TRCs leading to strong TETs) are realized mainly at high-amplitude regimes of the motion. Moreover, the variation of NES mass did not appear to affect the TET efficiency. Indeed, even for extremely small mass values, of the order of 0.04% of the plate mass, the NES efficiency was proved to remain robust (of the order of 70% of total input shock energy). This finding is significant from a practical point of view, as it shows that lightweight, essentially nonlinear attachments can indeed be designed as efficient passive shock absorbers, with minimal structural modification and mass addition to the system to be protected.

On the other hand, the variation of the damping coefficient of the NES affected significantly TET efficiency. In general, improved NES efficiency was achieved for relatively higher values of damping provided that the damping remained weak (strong damping would be disadvantageous to TET as it would restrict the capacity of the NES mass to achieve high relative displacements, so that the NES damper would not be efficient).

The parametric study of the input amplitude with stiffness restricted to the designed operating conditions of the plate shows that TETs are not affect so much and practically it is not a drawback the existence of the upper threshold beyond this level the TETs are getting very weak as showed in discrete cases so far.

In a continuation of the work by Georgiades et al. (2007), we showed that a combined Wavelet / EMD analysis is capable of identifying the strong nonlinear modal interactions that govern TETs in the system under examination. Specifically, we showed that TETs can be related to series of TRCs between IMFs of the responses of the plate and the SDOF NES; moreover, strong TETs were associated with TRCs occuring at the early, high-energy regime of the dynamics. This result is in agreement with the findings of Georgiades et al. (2007), where it was also shown that weak

TETs are associated with delayed TRCs occurring at energetically lower regimes of the dynamics. Hence, the outlined postprocessing approach is capable of identifying the main oscillatory components of strongly nonlinear time series, as well as, transient resonance interactions between them that give rise to strong energy exchanges between subsystems of a complex system.

The use of multiple SDOF NESs attached to the plate could enhance significantly weak TETs when NESs are attached at points close to nodal lines of plate modes. This is due to positive synergy between the NESs. Alternatively, MDOF NESs could be used instead of SDOF ones. It was shown that the TET efficiency of MDOF NESs is high only in cases of strong coupling with the plate; this is explained by noting that coupling stiffness must be sufficiently stiff in order to enable the MDOF NES to excite and engage in nonlinear resonance interactions a sufficiently large number of plate modes. The resulting TETs are broadband, as a significant set of plate modes engage in TRCs with the NNMs of the MDOF NES. Similarly to the SDOF NES case, when the MDOF NES is located at points close to nodal lines of plate modes, the nonlinear modal interactions between the NES and the plate are weak, and, as a result TET from the plate to the MDOF NES is also weak.

Therefore the optimal position for highest TETs of a single NES of any type is at the *antinodes of the linear modal analysis* of the structure.

A comparative study of the aforementioned NES configurations and the classical TMD showed the improved robustness of the nonlinear designs and that there is no preferable type of NES for shock isolation of the structure, as well as the faster rate of shock energy dissipation achieved for the nonlinear case. This is an expected finding, given that the NESs do not possess the single-tuning-frequency limitation of the TMD; instead, since they possess no preferential set of resonance frequencies and depending on their instantaneous energy, they are capable of engaging in TRC any plate mode (provided that that mode has no node close to the point of attachment to the NES), at wide frequency ranges. It is this capacity for broadband energy absorption that renders the NES an efficient and adaptive passive boundary controller. From a practical point of view, it is often encountered in engineering practice that due to fatigue or joint degradation the natural frequencies of a structure can gradually change, rendering attached TMDs inefficient; in such situations an NES would be able to still remain ‘tuned’ to structural modes and thus retain its efficiency, with no further design modification, moreover the TMD seems inappropriate to be used in case that the structure is subjected to multiple successive shocks. In additional considered problems involving aeroelastic flutter suppression (Lee et al., 2007), seismic mitigation (Nucera et al., 2007) and drill-string instability suppression (Viguie et al., 2007), the use of appropriately designed NESs was found to hold promise for a simple, passive, lightweight and robust solution.

Appendix-1

In this Appendix we show how the structural matrices arise from the discretization of the equations of motion (1). The element displacement vector, q_e, contains the 12 displacements (in the z-direction) and rotations (about the x- and y-axes) of the nodes of the elements; hence, q_e is a (12×1) vector defined as follows,

$$q_e = \begin{Bmatrix} q_i \\ q_j \\ q_k \\ q_l \end{Bmatrix}, \quad \text{e.g., } q_i = \begin{Bmatrix} w_i \\ \vartheta_{xi} \\ \vartheta_{yi} \end{Bmatrix} \text{ with } \vartheta_{xi} = \partial w / \partial y_i \,, \vartheta_{yi} = -\partial w / \partial x_i \tag{A.1}$$

Therefore, through the use of shape functions the distributed displacements and rotations at any position of an element, $w_e(x,y)$, can be expressed in terms of the displacements and rotations at the nodes of the element, as follows:

$$\begin{gathered} w_e = [N_i^1 \; N_i^2 \; N_i^3 \; N_j^1 \; N_j^2 \; N_j^3 \; N_k^1 \; N_k^2 \; N_k^3 \; N_l^1 \; N_l^2 \; N_l^3] \times \\ \begin{bmatrix} w_i & \vartheta_{xi} & \vartheta_{yi} & w_j & \vartheta_{xj} & \vartheta_{yj} & w_k & \vartheta_{xk} & \vartheta_{yk} & w_l & \vartheta_{xl} & \vartheta_{yl} \end{bmatrix}^T \Rightarrow \\ w_e = N \, q_e \end{gathered} \tag{A.2}$$

This expression defines the matrix of shape functions, N, for a single finite element of the type used herein.

The determination of the stiffness matrix, K_e^I, of a single FE can be performed using the strain energy E_{s,p_e} of that element, given by:

$$E_{s,p_e} = \frac{1}{2}\int_{V_e} \varepsilon_e^T \cdot H \cdot \varepsilon_e \, dV_e = \frac{1}{2}\int_{A_e}\int_{-h/2}^{h/2} \varepsilon_e^T \cdot H \cdot \varepsilon_e \, dA_e dz \Rightarrow E_{s,p_e} = \frac{1}{2} q_e^T \cdot K_e^I \cdot q_e \tag{A.3}$$

where,

$$H = \frac{E}{1-\nu^2}\begin{bmatrix} 1 & \nu & 0 \\ \nu & 1 & 0 \\ 0 & 0 & \dfrac{1-\nu}{2} \end{bmatrix} \tag{A.4}$$

and the strain ε_e within the element is defined from linear elasticity; using the Kirchoff assumptions the strain is expressed as,

$$\varepsilon_e = \begin{Bmatrix} \varepsilon_x \\ \varepsilon_y \\ \gamma_{xy} \end{Bmatrix} = -z_e \begin{Bmatrix} \partial^2/\partial x^2 \\ \partial^2/\partial y^2 \\ 2\cdot\partial^2/\partial x \partial y \end{Bmatrix} w_e = -z_e \cdot L \cdot w_e \tag{A.5}$$

In (A.5), $\varepsilon_x, \varepsilon_y$ and γ_{xy} are the components of the strain tensor, z_e is the z-coordinate within the element, and L is the operator,

$$L = \begin{Bmatrix} \partial^2/\partial x^2 \\ \partial^2/\partial y^2 \\ 2\cdot\partial^2/\partial x\partial y \end{Bmatrix} \tag{A.6}$$

Finally,

$$E_{s,p_e} = \frac{h^2}{24}\int_{A_e} q_e^T \cdot N^T \cdot L^T \cdot H \cdot L \cdot N \cdot q_e dA_e = \frac{1}{2} q_e^T \cdot K_e^I \cdot q_e \tag{A.7}$$

From equation (A.8) we define the stiffness matrix of the FE as follows:

$$K_e^I = \frac{h^2}{12}\int_{A_e} N^T \cdot L^T \cdot H \cdot L \cdot N\, dA_e \Rightarrow K_e^I \equiv \frac{E\cdot h^2}{12\cdot(1-\nu^2)} \begin{bmatrix} K_{1,1} & K_{1,2} & \cdots & K_{1,12} \\ K_{2,1} & K_{2,2} & \cdots & K_{2,12} \\ \vdots & \vdots & \ddots & \cdots \\ K_{12,1} & K_{12,2} & \cdots & K_{12,12} \end{bmatrix} \tag{A.8}$$

The explicit forms of the elements K_{ij} are presented in Appendix 2, by performing the required integrations in equation (A.8).

The determination of the mass matrix of the FE, M_e, can be performed employing the kinetic energy (E_{K,p_e}) of that element of the plate,

$$E_{K,p_e} \approx \frac{1}{2}\int_{V_e} \rho \cdot \dot{w}_e(x,y,t)^2 dV_e = \frac{1}{2} m_e \int_{A_e} \dot{w}_e(x,y,t)^2 dA_e \Rightarrow E_{K,p_e} \equiv \frac{1}{2}\dot{q}_e^T \cdot M_e \cdot \dot{q}_e \tag{A.9}$$

where,

$$m_e = \int_{-h/2}^{h/2} \rho dz_e = \rho h \tag{A.10}$$

and,

$$\dot{w}_e = \frac{dw_e}{dt} = N \cdot \dot{q}_e \tag{A.11}$$

Therefore, we express the kinetic energy of the FE as,

$$E_{K,p_e} \approx \frac{1}{2} m_e \int_{A_e} \dot{q}_e \cdot N^T \cdot N \cdot \dot{q}_e dA_e = \frac{1}{2}\dot{q}_e^T \cdot M_e \cdot \dot{q}_e \tag{A.12}$$

Finally, from equation (A.12) we define the Mass matrix for one plate element as follows:

$$M_e = m_e \int_{A_e} N^T \cdot N dA_e = m_e \begin{bmatrix} M_{1,1} & M_{1,2} & \cdots & M_{1,12} \\ M_{2,1} & M_{2,2} & \cdots & M_{2,12} \\ \vdots & \vdots & \ddots & \cdots \\ M_{12,1} & M_{12,2} & \cdots & M_{12,12} \end{bmatrix} \equiv m_e \cdot M_{elem} \tag{A.13}$$

The elements M_{ij} of the matrix M_{elem} are determined analytically in Appendix 2.

The determination of the stiffness matrix of the FE due to the elastic foundation, K_e^{II}, can be performed employing the dynamic energy, E_{u,p_e}, of that element of a plate:

$$E_{u,p_e} = \frac{1}{2} k \int_{A_e} w_e^2 dA_e \equiv \frac{1}{2} q_e^T \cdot K_e^{II} \cdot q_e \qquad (A.14)$$

The dynamic energy E_{u,p_e} is computed by,

$$E_{u,p_e} = \frac{1}{2} k \int_{A_e} w_e^2 \, dA_e = \frac{1}{2} k \int_{A_e} q_e^T \cdot N^T \cdot N \cdot q_e \, dA_e \Rightarrow E_{u,p_e} \equiv \frac{1}{2} q_e^T \cdot K_e^{II} \cdot q_e \quad (A.15)$$

Therefore, the stiffness matrix of the FE due to the elastic foundation is expressed as follows:

$$K_e^{II} = k \int_{A_e} N^T \cdot N \, dA_e = k \cdot M_{elem} \qquad (A.16)$$

The total stiffness matrix for each element $K_e^{I,II}$ is the sum of the matrices

$$K_e^{I,II} = K_e^I + K_e^{II} \qquad (A.17)$$

The determination of the damping matrix of the FE, Da_e, can be computed through the estimation of the energy dissipation of the plate defined as follows,

$$E_{dam,p_e} \approx \frac{1}{2} \int_0^t \int_{V_e} d \cdot \dot{w}_e^2(x,y,\tau) \cdot dV_e \, d\tau = \frac{1}{2} \int_0^t \dot{q}_e^T \cdot Da_e \cdot \dot{q}_e \, d\tau \qquad (A.18)$$

leading to the following expression:

$$D_e = d \cdot h \cdot \int_{A_e} N^T N \, dA_e = d \cdot h \cdot M_{elem} \qquad (A.19)$$

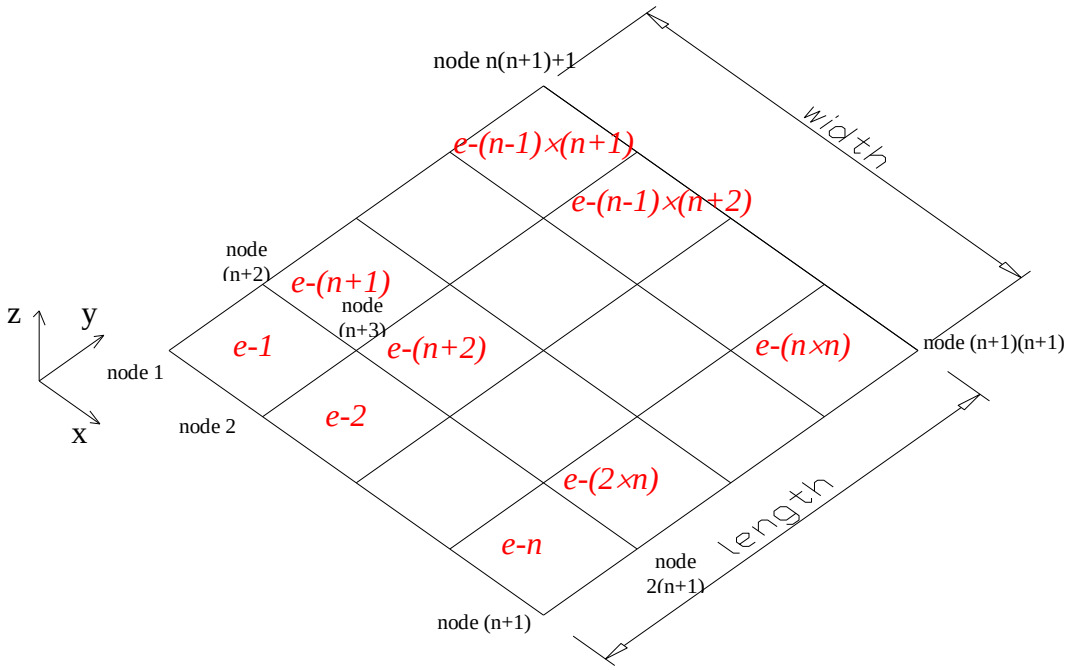

Figure A.1. Mesh of the plate; elements are labeled as e-p, p=1,…,(n×n), whereas nodes are numbered individually in the range [1,…,(n+1)×(n+1)].

Using the derived expressions for the mass, stiffness and damping matrices for the FE, we proceed to construct the full (global) matrices for the plate, that discretize the partial differential equation in equation (1). The matrix-ct (or connectivity table) is now formulated in order to divide the plate into a number of finite elements. This matrix defines the location of the nodes in the discrete plate, indicating the position of each node in terms of the global coordinates (x,y) positions, and the common nodes between adjacent elements (cf. Figure A.1).

The convention followed herein is that the x-positions correspond to the rows, and the y-positions to the columns of the ct-matrix corresponding to the plate discretization shown in Figure A.1. For example, position (x,y) at the plate corresponds the node defined by the (x/n+1)-row and (y/n+1)-column of the ct-matrix:

$$ct = \begin{bmatrix} 1 & n+2 & \cdots & n(n+1)+1 \\ 2 & n+3 & \vdots & \vdots \\ \vdots & \vdots & \vdots & \vdots \\ n+1 & 2(n+1) & \cdots & (n+1)(n+1) \end{bmatrix} \tag{A.20}$$

By using the ct-matrix and the elementary mass, stiffness and damping matrices defined previously we can construct the full (global) matrices of the plate and discretize the first equation in eq. (1) by summing up the elementary matrices as indicates the connectivity matrix for each node that correspond to many different elements. Finally we apply the boundary conditions by eliminating the nodes from the structural matrices that corresponds to the clamped end of the cantilever plate.

Appendix 2

Using the local coordinates and the shape functions defined in eq. (5-7) we obtain the following expressions,

$$
\begin{aligned}
&dx = \alpha d\xi \text{ with limits } (-1,1)\\
&dy = b d\eta \text{ with limits } (-1,1)\\
&\partial N/\partial x = \partial N/\partial \xi \; \partial \xi/\partial x = 1/\alpha \; \partial N/\partial \xi\\
&\partial^2 N/\partial x^2 = 1/\alpha^2 \; \partial^2 N/\partial \xi^2\\
&\partial N/\partial y = \partial N/\partial \eta \; \partial \eta/\partial y = 1/b \; \partial N/\partial \eta\\
&\partial^2 N/\partial y^2 = 1/b^2 \; \partial^2 N/\partial \eta^2\\
&\partial^2 N/\partial x \partial y = 1/\alpha \; 1/b \; \partial^2 N/\partial \xi \partial \eta
\end{aligned}
\qquad \text{(A.21)}
$$

where α and b are the dimensions of the element, and the coordinates of the nodes are,

Node i: $(\xi_i,\eta_i)=(-1,-1)$
Node j: $(\xi_j,\eta_j)=(1,-1)$
Node k: $(\xi_k,\eta_k)=(-1,1)$
Node l: $(\xi_l,\eta_l)=(1,1)$

The stiffness matrix of the plate is symmetrical, therefore it suffices to calculate its diagonal elements and the lower triagonal part of the matrix:

$$K_{1,1} = \frac{10\cdot\alpha^4 + 10\cdot b^4 + \alpha^2 b^2 (7-2\nu)}{10\cdot\alpha^3\cdot b^3},\; K_{2,1} = -\frac{1+\frac{10\alpha^2}{b^2}+4\nu}{10\alpha},\; K_{3,1} = \frac{1+\frac{10b^2}{\alpha^2}+4\nu}{10b},$$

$$K_{4,1} = \frac{5\cdot\alpha^4 - 10\cdot b^4 + \alpha^2 b^2 (-7+2\nu)}{10\cdot\alpha^3\cdot b^3},\; K_{5,1} = \frac{1-\frac{5\alpha^2}{b^2}+4\nu}{10\alpha},\; K_{6,1} = \frac{1+\frac{10b^2}{\alpha^2}-\nu}{10b},$$

$$K_{7,1} = \frac{-10\cdot\alpha^4 + 5\cdot b^4 + \alpha^2 b^2 (-7+2\nu)}{10\cdot\alpha^3\cdot b^3},\; K_{8,1} = \frac{-1-\frac{10\alpha^2}{b^2}+\nu}{10\alpha},\; K_{9,1} = \frac{-1+\frac{5b^2}{a^2}-4\nu}{10b},$$

$$K_{10,1} = \frac{-10\cdot\alpha^4 - 5\cdot b^4 + \alpha^2 b^2 (7-2\nu)}{10\cdot\alpha^3\cdot b^3},\; K_{11,1} = -\frac{5\alpha^2 + b^2(-1+\nu)}{10\alpha b^2},$$

$$K_{12,1} = \frac{5b^2 + \alpha^2(-1+\nu)}{10\alpha^2 b},\; K_{2,2} = \frac{4(5\cdot\alpha^4 - b^2(-1+\nu))}{15\cdot\alpha b},\; K_{4,2} = \frac{1-\frac{5\alpha^2}{b^2}+4\nu}{10\alpha},$$

$$K_{5,2} = \frac{10\alpha^2 + 4b^2(-1+\nu)}{15\alpha b},\; K_{7,2} = \frac{1+\frac{10\alpha^2}{b^2}-\nu}{10\alpha},\; K_{8,2} = \frac{10\alpha^2 + b^2(-1+\nu)}{10\alpha b},$$

$$K_{10,2} = \frac{5\alpha^2 + b^2(-1+\nu)}{10\alpha b^2},\; K_{11,2} = \frac{5\alpha^2 + b^2(1-\nu)}{15\alpha b},\; K_{3,3} = \frac{4(5b^2 - \alpha^2(-1+\nu))}{15\alpha b},$$

$$K_{4,3} = \frac{-1-\frac{10b^2}{\alpha^2}+\nu}{10b},\; K_{6,3} = \frac{10b^2 + \alpha^2(-1+\nu)}{15\alpha b},\; K_{7,3} = \frac{-1+\frac{5b^2}{\alpha^2}-4\nu}{10b},$$

$$K_{9,3}=\frac{10b^2+\alpha^2(-1+\nu)}{15\alpha b},\ K_{10,3}=-\frac{5b^2+\alpha^2(-1+\nu)}{10\alpha^2 b},\ K_{12,3}=\frac{\alpha^2+5b^2-\alpha^2\nu}{15\alpha b},$$

$$K_{4,4}=\frac{10\cdot\alpha^4+10\cdot b^4+\alpha^2b^2(7-2\nu)}{10\cdot\alpha^3\cdot b^3},\ K_{5,4}=-\frac{1+\frac{10\alpha^2}{b^2}+4\nu}{10\alpha},\ K_{6,4}=-\frac{1+\frac{10b^2}{\alpha^2}+4\nu}{10b},$$

$$K_{7,4}=\frac{-5\cdot\alpha^4-5\cdot b^4+\alpha^2b^2(7-2\nu)}{10\cdot\alpha^3\cdot b^3},\ K_{8,4}=-\frac{5\alpha^2+5b^2(-1+\nu)}{10\alpha b^2},$$

$$K_{9,4}=-\frac{5b^2+\alpha^2(-1+\nu)}{10\alpha^2 b},\ K_{10,4}=\frac{-10\cdot\alpha^4+5\cdot b^4+\alpha^2b^2(-7+2\nu)}{10\cdot\alpha^3\cdot b^3},$$

$$K_{11,4}=\frac{-1-\frac{10\alpha^2}{b^2}+\nu}{10\alpha},\ K_{12,4}=\frac{1-\frac{5b^2}{\alpha^2}+4\nu}{10b},\ K_{5,5}=\frac{4(5\alpha^2-b^2(-1+\nu))}{15\alpha b},$$

$$K_{7,5}=\frac{5\alpha^2+b^2(-1+\nu)}{10\alpha b^2},\ K_{8,5}=\frac{5\alpha^2+b^2(1-\nu)}{15\alpha b},\ K_{10,5}=\frac{1+\frac{5\alpha^2}{b^2}-\nu}{10\alpha},$$

$$K_{11,5}=\frac{10\alpha^2+b^2(-1+\nu)}{15\alpha b},\ K_{6,6}=\frac{4(5b^2-\alpha^2(-1+\nu))}{15\alpha b},\ K_{7,6}=\frac{5b^2+\alpha^2(-1+\nu)}{10\alpha^2 b},$$

$$K_{9,6}=\frac{\alpha^2+5b^2-\alpha^2\nu}{15\alpha b},\ K_{10,6}=\frac{1-\frac{5b^2}{\alpha^2}+4\nu}{10b},\ K_{12,6}=\frac{10b^2+4\alpha^2(-1+\nu)}{15\alpha b},$$

$$K_{7,7}=\frac{10\cdot\alpha^4+10\cdot b^4+\alpha^2b^2(7-2\nu)}{10\cdot\alpha^3\cdot b^3},\ K_{8,7}=\frac{1+\frac{10\alpha^2}{b^2}+4\nu}{10\alpha},\ K_{9,7}=\frac{1+\frac{10b^2}{\alpha^2}+4\nu}{10b},$$

$$K_{10,7}=\frac{5\cdot\alpha^4-10\cdot b^4+\alpha^2b^2(-7+2\nu)}{10\cdot\alpha^3\cdot b^3},\ K_{11,7}=\frac{-1+\frac{5\alpha^2}{b^2}-4\nu}{10\alpha},\ K_{12,7}=\frac{1+\frac{10b^2}{\alpha^2}-\nu}{10b},$$

$$K_{8,8}=\frac{4(5\alpha^2-b^2(-1+\nu))}{15\alpha b},\ K_{10,8}=\frac{-1+\frac{5\alpha^2}{b^2}-4\nu}{10\alpha},\ K_{11,8}=\frac{10\alpha^2+4b^2(-1+\nu)}{15\alpha b},$$

$$K_{9,9}=\frac{4(5b^2-\alpha^2(-1+\nu))}{15\alpha b},\ K_{10,9}=\frac{-1-\frac{10b^2}{\alpha^2}+\nu}{10b},\ K_{12,9}=\frac{10b^2+\alpha^2(-1+\nu)}{15\alpha b},$$

$$K_{10,10}=\frac{10\cdot\alpha^4+10\cdot b^4+\alpha^2b^2(7-2\nu)}{10\cdot\alpha^3\cdot b^3},\ K_{11,10}=\frac{1+\frac{10\alpha^2}{b^2}+4\nu}{10\alpha},\ K_{12,10}=-\frac{1+\frac{10b^2}{\alpha^2}+4\nu}{10b},$$

$$K_{11,11}=\frac{4(5\alpha^2-b^2(-1+\nu))}{15\alpha b},\ K_{12,12}=\frac{4(5b^2-\alpha^2(-1+\nu))}{15\alpha b},$$

$$K_{6,2}=K_{9,2}=K_{12,2}=K_{9,5}=K_{5,3}=K_{8,3}=K_{11,3}=K_{12,8}=K_{11,9}=K_{12,5}=K_{8,6}=K_{11,6}=0,$$

$$K_{3,2}=K_{12,11}=-\nu,\ K_{9,8}=K_{6,5}=\nu \qquad \text{(A-22)}$$

The M_{el} matrix is symmetrical, therefore, it suffices to calculate the diagonal elements and the upper triangular part of the matrix:

$$M_{1,1}=\frac{1727\alpha b}{3150},\ M_{1,2}=-\frac{461\alpha b^2}{3150},\ M_{1,3}=\frac{461\alpha^2 b}{3150},\ M_{1,4}=\frac{613\alpha b}{3150},\ M_{1,5}=-\frac{199\alpha b^2}{3150},$$

$$M_{1,6}=-\frac{137\alpha^2 b}{1575},\ M_{1,7}=\frac{613\alpha b}{3150},\ M_{1,8}=\frac{137\alpha b^2}{1575},\ M_{1,9}=\frac{199\alpha^2 b}{3150},\ M_{1,10}=\frac{197\alpha b}{3150},$$

$$M_{1,11}=\frac{58\alpha b^2}{1575},\ M_{1,12}=-\frac{58\alpha^2 b}{1575},\ M_{2,2}=\frac{16\alpha b^3}{315},\ M_{2,3}=-\frac{\alpha^2 b^2}{25},\ M_{2,4}=-\frac{199\alpha b^2}{3150},$$

$$M_{2,5}=\frac{8\alpha b^3}{315},\ M_{2,6}=\frac{2\alpha^2 b^2}{75},\ M_{2,7}=-\frac{137\alpha b^2}{1575},\ M_{2,8}=-\frac{4\alpha b^3}{105},\ M_{2,9}=-\frac{2\alpha^2 b^2}{75},$$

$$M_{2,10}=-\frac{58\alpha b^2}{1575},\ M_{2,11}=-\frac{2\alpha b^3}{105},\ M_{2,12}=\frac{4\alpha^2 b^2}{225},\ M_{3,3}=\frac{16\alpha^3 b}{315},\ M_{3,4}=\frac{137\alpha^2 b}{1575},$$

$$M_{3,5}=-\frac{2\alpha^2 b^2}{75},\ M_{3,6}=-\frac{4\alpha^3 b}{105},\ M_{3,7}=\frac{199\alpha^2 b}{3150},\ M_{3,8}=\frac{2\alpha^2 b^2}{75},\ M_{3,9}=\frac{8\alpha^3 b}{315},$$

$$M_{3,10}=\frac{58\alpha^2 b}{1575},\ M_{3,11}=\frac{4\alpha^2 b^2}{225},\ M_{3,12}=-\frac{2\alpha^3 b}{105},\ M_{4,4}=\frac{1727\alpha b}{3150},\ M_{4,5}=-\frac{461\alpha b^2}{3150},$$

$$M_{4,6}=-\frac{461\alpha^2 b}{3150},\ M_{4,7}=\frac{197\alpha b}{3150},\ M_{4,8}=\frac{58\alpha b^2}{1575},\ M_{4,9}=\frac{58\alpha^2 b}{1575},\ M_{4,10}=\frac{613\alpha b}{3150},$$

$$M_{4,11}=\frac{137\alpha b^2}{1575},\ M_{4,12}=-\frac{199\alpha^2 b}{3150},\ M_{5,5}=\frac{16\alpha b^3}{315},\ M_{5,6}=\frac{\alpha^2 b^2}{25},\ M_{5,7}=-\frac{58\alpha b^2}{1575},$$

$$M_{5,8}=-\frac{2\alpha b^3}{105},\ M_{5,9}=-\frac{4\alpha^2 b^2}{225},\ M_{5,10}=-\frac{137\alpha b^2}{1575},\ M_{5,11}=-\frac{4\alpha b^3}{105},\ M_{5,12}=\frac{2\alpha^2 b^2}{75},$$

$$M_{6,6}=\frac{16\alpha^3 b}{315},\ M_{6,7}=-\frac{58\alpha^2 b}{1575},\ M_{6,8}=-\frac{4\alpha^2 b^2}{225},\ M_{6,9}=-\frac{2\alpha^3 b}{105},\ M_{6,10}=-\frac{199\alpha^2 b}{3150},$$

$$M_{6,11}=-\frac{2\alpha^2 b^2}{75},\ M_{6,12}=\frac{8\alpha^3 b}{315},\ M_{7,7}=\frac{1727\alpha b}{3150},\ M_{7,8}=\frac{461\alpha b^2}{3150},\ M_{7,9}=\frac{461\alpha^2 b}{3150},$$

$$M_{7,10}=\frac{613\alpha b}{3150},\ M_{7,11}=\frac{199\alpha b^2}{3150},\ M_{7,12}=-\frac{137\alpha^2 b}{1575},\ M_{8,8}=\frac{16\alpha b^3}{315},\ M_{8,9}=\frac{\alpha^2 b^2}{25},$$

$$M_{8,10}=\frac{199\alpha b^2}{3150},\ M_{8,11}=\frac{8\alpha b^3}{315},\ M_{8,12}=-\frac{2\alpha^2 b^2}{75},\ M_{9,9}=\frac{16\alpha^3 b}{315},\ M_{9,10}=\frac{137\alpha^2 b}{1575},$$

$$M_{9,11}=\frac{2\alpha^2 b^2}{75},\ M_{9,12}=-\frac{4\alpha^3 b}{105},\ M_{10,10}=\frac{1727\alpha b}{3150},\ M_{10,11}=\frac{461\alpha b^2}{3150},\ M_{10,12}=-\frac{461\alpha^2 b}{3150},$$

$$M_{11,11}=\frac{16\alpha b^3}{315},\ M_{11,12}=-\frac{\alpha^2 b^2}{25},\ M_{12,12}=\frac{16\alpha^3 b}{315} \qquad \text{(A-23)}$$

REFERENCES

Den Hartog J.P., [1947], *Mechanical Vibration,* McGraw-Hill, New York.

Frahm H., [1911], 'A Device for Damping Vibration of Bodies', US Patent 989958.

Gendelman, O., Manevitch, L.I., Vakakis, A.F., and M'Closkey, R. [2001], 'Energy 'Pumping' in Coupled Mechanical Oscillators I: Dynamics of the Underlying Hamiltonian Systems,' *ASME J. Appl. Mech*., **68**, 34-41.

Georgiades F., A.F. Vakakis [2007], 'Dynamics of a Linear Beam with an Attached Local Nonlinear Energy Sink,' *Communications in Nonlinear Science and Numerical Simulation*, **12** (5), 643-561.

Georgiades F., Vakakis A.F., Kerschen G. [2007], 'Broadband Passive Targeted Energy Pumping From a Linear Dispersive Rod to a Lightweight Essentially Nonlinear End Attachment,' *Int. Journal of Nonlinear Mechanics*, **42** (1), 36-57.

Georgiades F. [2006], *'Nonlinear Localization and Targeted Energy Transfer Pheonomena in Vibrating Systems with Smooth and Non-Smooth Stiffness Nonlinearities,*' Ph.D. Thesis, National Technical University of Athens, Greece.

Gerandin M., Rixen D. [1997], *Mechanical Vibrations, Theory and Application to Structural Dynamics,* John Willey & Sons, New York.

Huang N.E., Z. Shen, S.R. Long, M.C. Wu, H.H. Shih, Q. Zheng, N.C. Yen, C.C. Tung, H.H. Liu [1998], 'The Empirical Mode Decomposition and the Hilbert Spectrum for Nonlinear and Non-stationary Time Series Analysis,' *Proceedings of the Royal Society of London, Series A*, **454**, 903-995.

Huang N.E., M.C. Wu, S.R. Long, S.S.P. Shen, W. Qu, P. Gloersen, K.L. Fan [2003], 'A Confidence Limit for the Empirical Mode Decomposition and Hilbert Spectral Analysis,' *Proceedings of the Royal Society of London, Series A*, **459**, 2317-2345.

Kerschen G., Lee Y.S., Vakakis A.F., McFarland D.M., Bergman L.A. [2005], 'Irreversible Passive Energy Transfer in Coupled Oscillators with Essential Nonlinearity,' *SIAM Journal on Applied Mathematics,* **66** (2), 648-679.

Lee Y.S., Kerschen G., Vakakis A.F., Panagopoulos P.N., Bergman L.A., McFarland D.M. [2005], 'Complicated Dynamics of a Linear Oscillator with a Light, Essentially Nonlinear Attachment,' *Physica D,* **204** (1-2), 41-69.

Lee Y.S., Vakakis A.F., Bergman L.A., McFarland D.M., Kerschen G. [2007], 'Suppression of Aeroelastic Instability by Means of Broadband Passive Targeted Energy Transfers, Part I: Theory,' *AIAA Journal*, **45** (3), 693-711.

Leissa A., [1993], *Vibration of Plates,* Acoustical Society of America Publication.

Liu G.r., Quek S.S. [2003], *The Finite Element Method: A Practical Course*,' Butteworth-Heinemann, Oxford.

Melosh R.J. [1963], 'Structural Analysis of Solids,' *ASCE Structural Journal,* **4**, 205-223.

Nucera F., McFarland D.M., Bergman L.A., Vakakis A.F. [2007], 'Application of Broadband Nonlinear Targeted Energy Transfers for Seismic Mitigation of a Shear Frame: Part I. Computational Results; Part II. Experimental Results,' *Journal of Sound and Vibration* (submitted).

Tsakirtzis S., Kerschen G., Panagopoulos P., Vakakis A.F. [2005], 'Multi-frequency Nonlinear Energy Transfer from Linear Oscillators to MDOF Essentially Nonlinear Attachments,' *Journal of Sound and Vibration,* **285**, 483-490.

Tsakirtzis S., Panagopoulos P., Kerschen G., Gendelman O., Vakakis A.F., Bergman L.A. [2007], 'Complex Dynamics and Targeted Energy Transfer in Linear Oscillators Coupled to Multi-degree-of-freedom Essentially Nonlinear Attachments,' *Nonlinear Dynamics* **48**, pp. 285-318.

Vakakis A.F. [2001], 'Inducing Passive Nonlinear Energy Sinks in Linear Vibrating Systems,' *Journal of Vibration and Acoustics,* **123** (3), 324-332.

Vakakis A.F. and Gendelman O. [2001], 'Energy Pumping in Nonlinear Mechanical Oscillators II: Resonance Capture,' *Journal of Applied Mechanics,* **68** (1), 42-48.

Vakakis A.F., Manevitch L.I., Mikhlin Yu.V., Pilipchuk V.N., Zevin A.A. [1996], *Normal Modes and Localization in Nonlinear Systems*, J. Wiley & Sons.

Veltcheva A.D., C.G. Soares [2004], 'Identification of the Components of Wave Spectra by the Hilbert Huang Transform Method,' *Applied Ocean Research,* **26**, 1-12.

Viguie R., Kerschen G., Golinval J.C., McFarland D.M., Bergman L.A., Vakakis A.F., Van de Wouw N. [2007], 'Using Passive Nonlinear Targeted Energy Transfer to Stabilize Drill-String Systems,' *Journal of Mechanical Systems and Signal Processing* (in press).

Zienkiewicz O.C., Taylor R.L. (5^{th} ed.) [2000], *The Finite Element Method, Volume 2: Solid Mechanics*, Butteworth-Heinemann, Oxford.

Zhang R.R., R. King, L. Olson, Y.-L. Xu [2005], 'Dynamic Response of the Trinity River Relief Bridge to Controlled Pile Damage: Modeling and Experimental Data Analysis Comparing Fourier and Hilbert-Huang Techniques,' *Journal of Sound and Vibration*, **285**, 1049-1070.